journal of
thrombosis and haemostasis

Quantitative super-resolution imaging of platelet degranulation reveals differential release of VWF and VWF propeptide from alpha-granules

Journal:	*Journal of Thrombosis and Haemostasis*
Manuscript ID	JTH-2022-01221.R1
Article Type:	Original Article
Date Submitted by the Author:	10-Mar-2023
Complete List of Authors:	Swinkels, Maurice; Erasmus Medical Center, Hematology Hordijk, Sophie; Erasmus MC, Hematology Bürgisser, Petra; Erasmus MC, Hematology Slotman, Johan A.; Erasmus Medical Center, Optical Imaging Center, Department of Pathology Carter, Tom; St Georges University, CVCSRI Leebeek, Frank; Erasmus Univ. Medical center, Hematology Jansen, A.J. Gerard; Erasmus MC, Department of Hematology, Voorberg, Jan; Sanquin Research, Molecular Hematology Bierings, Ruben; Erasmus MC, Hematology;
Key Words:	von Willebrand factor, exocytosis, blood platelets, hemostasis, Secretory Vesicles

Quantitative super-resolution imaging of platelet degranulation reveals differential release of VWF and VWF propeptide from alpha-granules.

Running title: Differential release of platelet alpha-granule cargo

Maurice Swinkels[1*], Sophie Hordijk[1*], Petra E. Bürgisser[1], Johan A. Slotman[2], Tom Carter[3], Frank W.G. Leebeek[1], A.J. Gerard Jansen[1], Jan Voorberg[4,5] and Ruben Bierings[1]

[1]Department of Hematology and [2]Optical Imaging Center, Department of Pathology, Erasmus MC, University Medical Center Rotterdam, Rotterdam, The Netherlands; [3]Molecular and Clinical Sciences Research Institute, St George's University of London, United Kingdom; [4]Molecular Hematology, Sanquin Research and Landsteiner Laboratory, Amsterdam University Medical Center, University of Amsterdam, The Netherlands; [5]Experimental Vascular Medicine, Amsterdam University Medical Center, University of Amsterdam, The Netherlands.

[*]These authors contributed equally to this work

Corresponding author:

Dr. Ruben Bierings, Department of Hematology, Erasmus MC, University Medical Center Rotterdam, The Netherlands. e-mail: r.bierings@erasmusmc.nl

Word count abstract:	248	Figure count:	5
Word count main body:	4386	Table count:	0
References: 67			

Key points:

1) VWFpp and VWF are localized in the same, eccentric alpha-granule subdomain in resting platelets

2) VWFpp and VWF are differentially secreted from individual alpha-granules upon activation with platelet agonists PAR-1 activating peptide and collagen-related peptide

Abstract

Background: Von Willebrand factor (VWF) and the VWF propeptide (VWFpp) are stored in eccentric nanodomains within platelet alpha-granules. VWF and VWFpp can undergo differential secretion following Weibel-Palade body (WPB) exocytosis in endothelial cells, however, it is unclear if the same process occurs during platelet alpha-granule exocytosis. Using a high-throughput 3D super-resolution imaging workflow for quantification of individual platelet alpha-granule cargo we have studied alpha-granule cargo release following platelet activation.

Aims: To investigate how VWF and VWFpp are released from alpha-granules in response to physiological stimuli.

Methods: Platelets were activated with PAR-1 activating peptide (PAR-1 ap) or collagen-related peptide (CRP-XL). Alpha-tubulin, VWF, VWFpp, SPARC and fibrinogen were imaged using 3D-SIM, followed by semi-automated analysis in FIJI. Uptake of anti-VWF nanobody during degranulation was used to identify alpha-granules that partially released content.

Results:

VWFpp overlapped with VWF in eccentric alpha-granule subdomains in resting platelets and showed a higher degree of overlap than SPARC or fibrinogen. Activation of PAR-1 or GPVI signaling caused a dose-dependent increase in alpha-granule exocytosis. More than 80% of VWF+ alpha-granules were retained, even at the highest agonist concentration used (20 μM PAR-1 ap). In contrast, the fraction of alpha-granules containing VWFpp decreased in a dose-dependent manner to 23%, whilst SPARC and fibrinogen were still detected in 60-70%. Similar results were obtained using CRP-XL. Anti-VWF nanobody was taken up by VWF+/VWFpp- structures and increased with stimulus strength, demonstrating these were post-exocytotic structures.

Conclusions: We provide evidence for differential secretion of VWF and VWFpp from individual alpha-granules.

Introduction

During thrombopoiesis several types of secretory granules from bone marrow megakaryocytes are packaged into budding platelets. Release of their content enables platelets to rapidly respond to changes in their environment, such as during injury, inflammation or when encountering pathogens. Alpha-granules are the most abundant platelet secretory organelle, and contain various proteins and molecules involved in the hemostatic response [1,2]. Among these is von Willebrand Factor (VWF), a key hemostatic adhesive glycoprotein whose main roles are to facilitate platelet adhesion to sites of vascular injury and to stabilize coagulation factor VIII in the circulation [3]. VWF is also made by endothelial cells and stored in Weibel-Palade bodies (WPBs) where it can be released via exocytosis following cellular activation. Circulating VWF levels in plasma are primarily maintained through basal secretion of WPBs from the endothelium [4].

Our knowledge on VWF biosynthesis primarily comes from studies utilizing endothelial cells and heterologous expression systems as cellular models. As it progresses through the secretory pathway, VWF undergoes several post-translational processing steps which include dimerization, glycosylation and multimerization into long platelet-adhesive concatemers [3]. Within the acidifying milieu of the Golgi, VWF multimers condense into helical VWF tubules that lend the WPBs their characteristic rod-like shape [5]. Here, a large N-terminal moiety called the VWF propeptide (VWFpp), is proteolytically cleaved from the mature VWF chain. In endothelial cells, cleaved VWFpp remains non-covalently associated with VWF due to the prevailing conditions in the Golgi and beyond (low pH, high Ca^{2+}), leading to its co-packaging in the forming WPBs [6–8]. VWFpp is essential for VWF multimerization, tubulation and WPB biogenesis [9–11] and becomes an integral part of the VWF tubules *in vitro* and *in vivo*

[12,13]. During exocytosis, the vesicle interior neutralizes leading to the rapid decondensation of VWF tubules [14,15] and loss of the non-covalent association between VWF and VWFpp [16]. Depending on the type of exocytosis (full fusion, lingering kiss or compound fusion) [4] and the extracellular environment, VWF, VWFpp and other WPB cargo molecules undergo divergent fates post-release [16–19].

In platelets VWF is zonally packaged within eccentric alpha-granule nanodomains, which also contain short VWF tubules [20–22], and can be released upon stimulus [23]. Platelets also contain VWFpp [24] and are able to secrete the protein following stimulation with various agonists that induce alpha-granule release [25]. However, the organization of VWFpp in alpha-granules or its release from alpha-granules have not been documented in detail. Similar to endothelial WPBs, platelet alpha-granules can undergo single and compound exocytosis depending on the type and magnitude of stimulus [26,27]. Following activation, alpha-granule cargo such as VWF, fibrinogen as well as chemokines and other mediators are not released uniformly, but can vary significantly between proteins in terms of release kinetics and in the proportions that are released or retained after degranulation [28–30]. Many of these cargo proteins are non-homogenously distributed within alpha-granules [22,29,31–33], which has led to the hypothesis that their differential release is the result of uneven solubilization of alpha-granule cargo clusters [28]. It is not clear how these processes influence the efficiency of release of VWF and VWFpp specifically, or whether VWF and VWFpp release from platelet alpha-granules is comparable to their release from endothelial cell storage organelles.

In this study we have investigated the storage and release of VWF and VWFpp in platelets using 3D Structured Illumination Microscopy (3D-SIM). We show that VWF and VWFpp reside in a distinct alpha-granule subdomain not occupied by other alpha-

granule proteins such as fibrinogen. By quantitative 3D-SIM analysis of residual VWF and VWFpp in activated platelets we demonstrate that VWFpp is efficiently released from platelets in a dose-dependent manner, while even at maximal activation the bulk of VWF remains associated with platelets in post-fusion structures. Our study sheds new light on the divergent outcomes of VWF and VWFpp following release from platelet alpha-granules.

Methods

Platelet isolation

All steps are carried out at room temperature (RT) unless otherwise stated. Whole blood is drawn from consenting healthy donors in citrate tubes. Washed platelets were prepared as described previously [22]. In brief, platelet-rich plasma (PRP) is generated by centrifugation at 120 x g for 20 minutes with low acceleration (max. 5) and low brake (max. 3). PRP is washed once in 10% acid-citrate dextrose buffer (85 mM Na_3-citrate, 71 mM citric acid, 111 mM glucose) with 111 µM prostaglandin E_1 (Sigma), twice in washing buffer (36 mM citric acid, 103 mM NaCl, 5 mM KCl, 5 mM EDTA, 5.6 mM glucose, pH 6.5) with 11 and 0 µM prostaglandin E_1 respectively, then resuspended at 250*10^3 platelets/µL in assay buffer (10 mM HEPES, 140 mM NaCl, 3 mM KCl, 0.5 mM $MgCl_2$, 10 mM glucose and 0.5 mM $NaHCO_3$, pH 7.4).

Platelet activation

Washed platelets at 250*10^3 platelets/µL were stimulated with 0-20 µM of PAR-1 activating peptide (Peptides International) or 0-1 µg/ml collagen-related peptide (CRP-XL, CambCol Labs) for 30 minutes at 37 ºC. Reactions are stopped by adding 1% paraformaldehyde (final concentration) for 5 minutes, then quenched with 50 mM NH_4Cl for 5 minutes. Samples are diluted in a large volume of washing buffer, washed once, and resuspended in assay buffer at approximately 250*10^3/µL.

VWF nanobody internalization assay

Washed platelets were incubated with nanobodies directed against the VWF CTCK domain or control nanobodies (s-VWF and R2), respectively [34]; kindly supplied by Dr. Coen Maas, UMCU, Netherlands) at a final concentration of 1 µg/ml and were

stimulated as described above. Internalized nanobodies were detected using goat anti-Alpaca IgG-AF488 (Jackson ImmunoResearch).

Flow cytometry

Small aliquots are taken for quality control of platelet activation by flow cytometry. Samples are stained with CD61-APC (BD Biosciences, 1:400) and CD62P-PE (BD Biosciences, 1:100) or with secondary anti-Alpaca IgG-AF488 (Jackson ImmunoResearch, 1:400) for 15 minutes at RT, diluted in assay buffer, and immediately read on a FACS Canto II flow cytometer (BD Biosciences). In some cases fixed platelets were permeabilized with 0.05% saponin before staining. FSC and SSC parameters were used to gate platelets and single cells, while single stains and isotype controls were used to determine fluorescence gating.

Platelet seeding and immunofluorescence

Seeding and staining was performed as described previously [22]. In brief, all unique sample conditions were seeded on poly-D-lysine coated 9 mm diameter 1.5H high-precision coverslips (Marienfeld), permeabilized, and stored in PGAS (0.2% gelatin, 0.02% azide and 0.02% saponin in PBS). Primary and secondary antibody staining were done in PGAS for 30 minutes at RT, washed 3x with PGAS following incubations. Antibodies used are listed in Supplementary Table S1. Finally, slides were dipped in PBS, mounted in Mowiol and imaged within one week.

Structured illumination- and confocal microscopy and image analysis

All samples were imaged with SIM (Elyra PS.1, Zeiss) and confocal microscopy (SP8, Leica). Three representative fields of view were collected per donor, using 40 Z-slices with an interval of 110 nm (4.4 µm in total). Raw SIM images were reconstructed with

state-of-the-art Zen Software (Zeiss). Due to very bright alpha-tubulin signals and relatively broad emission filters crosstalk between the far-red and red channel was observed, which was corrected equally in all applicable images by subtracting the far-red channel (alpha-tubulin) from the red channel. The number of 3D granular structures per platelet were separately quantified for VWF, VWFpp, SPARC and Fbg. SIM images were analyzed through ImageJ-based processing workflows as described in detail previously [20]. In brief, individual platelets were segmented based on alpha-tubulin staining, and individual 2D and 3D granular structures were quantified based on individual staining (e.g. VWF/VWFpp) by automated thresholding. Platelets in which 2D and 3D granule counts within the same channel differed by more than 15 were excluded from the analysis. Colocalization parameters were determined using the ColocThreshold FIJI plugin [35] (macro script available at https://github.com/Clotterdam/Swinkels-et-al-2023).

For analyzing the nanobody internalization assay, images without alpha-tubulin were segmented in individual platelets based on local differences in signal intensity using in-house written macro code (script available at GitHub as linked above). VWF+ granules were identified with the 3D Object Counter [36] and were converted into a mask in which the presence of VWFpp and/or VWF nanobody was measured.

Immunoblotting

HUVECs (grown as previously described [37]) and washed platelets were lysed in NP-40 buffer (0.5% NP-40, 150 mM NaCl, 10 mM Tris, 5 mM EDTA, pH 8.5). Lysate samples, normalized for VWF concentration, were separated on 4-12% Bis-Tris NuPAGE gels (Invitrogen) under reducing conditions and transferred to 0.2 µm nitrocellulose membranes. Membranes were probed with rabbit anti-VWF (DAKO) and

rabbit anti-VWFpp [19] followed by LT680-labeled donkey anti-rabbit secondary antibodies (Li-COR). Membranes were scanned on an Odyssey scanner (Li-COR).

Platelet secretion assay and VWF and VWFpp ELISA

Washed platelets ($5.6*10^6$ platelets in final volume of 200 µL) of 4 independent healthy donors were stimulated with 0-20 µM of PAR-1 activating peptide (Peptides International) or 0-1 µg/ml collagen-related peptide (CRP-XL, CambCol Labs) for 30 minutes at 37 ºC. Releasates and platelets were separated by centrifugation (13000 g), after which platelet pellets were lysed in 50 µL lysis buffer (1% Triton X-100, 10% glycerol, 50 mM Tris-HCL, 100 mM NaCl, 1mM EDTA, pH 7.4). VWF and VWFpp secretion were determined by sandwich ELISA as described earlier [38], using rabbit polyclonal anti-human VWF (DAKO; 0.5 µg/well) or mouse monoclonal anti-human VWFpp (CLB-Pro35; 1.0 µg/well) as coating antibodies and HRP-conjugated rabbit polyclonal anti-human VWF (DAKO; 0.5 µg/ml) or HRP-conjugated mouse monoclonal anti-human VWFpp (CLB-Pro14-3; 0.125 µg/ml), respectively, for detection. Blocking, washing and detection steps were performed in TWEB buffer (0.1% Tween-20, 0.2% gelatin, and 1 mM EDTA in PBS). HRP activity was measured by colorimetric detection of 3,3',5,5'-tetramethylbenzidine conversion using a Victor X4 microplate reader (Perkin Elmer). All samples were measured in 3 different dilutions in duplicate. Concentrated conditioned media from HEK293Ts stably expressing human wildtype VWF and VWFpp [39], which was calibrated against a normal plasma pool of >30 donors, was used as a standard.

Statistical analysis

Individual stimulation conditions were compared with resting platelets by two-way ANOVA. Multiple comparisons were corrected using Sidak's multiple comparisons test.

All statistical analyses were performed with GraphPad Prism (version 8). Data is presented as mean ± 95% confidence interval unless stated otherwise. A p-value under 0.05 was considered statistically significant.

Results

VWFpp colocalizes with mature VWF in eccentric alpha-granule nanodomains

The localization of VWF and VWFpp in resting platelets was studied by 3D-SIM [22]. VWF- and VWFpp-immunoreactivity were localized to discrete regions within the platelet (Figure 1A, Supplemental Figure 1) that were encapsulated by a P-selectin positive membrane (Supplemental Figure 2). Together with the presence of SPARC and fibrinogen these regions were identified as alpha-granules within the platelet cytoplasm (Figure 1B-C). Consistent with previous ultrastructural studies [18–20,31] close inspection of our images showed that VWF and VWFpp were co-located in a subdomain within the alpha-granule (Figure 1A), whilst SPARC or fibrinogen showed a more homogenous distribution and appear to be excluded from these VWF containing nanodomains (Figure 1B-C). Co-localization analysis confirmed the striking overlap between VWF- and VWFpp-immunoreactivity within individual alpha-granules (PCC_{VWFpp}: 0.521; $MCC1_{VWFpp}$: 0.590, $MCC2_{VWFpp}$: 0.548), (Figure 1D), whilst the overlap between VWF- and SPARK or fibrinogen, was as expected, lower (SPARC; PCC_{SPARC}: 0.336; $MCC1_{SPARC}$: 0.386, $MCC2_{SPARC}$: 0.498. Fibrinogen; $PCC_{Fibrinogen}$: 0.369; $MCC1_{Fibrinogen}$: 0.467, $MCC2_{Fibrinogen}$: 0.571) (Figure 1D-E). In these experiments a rabbit polyclonal antibody that specifically recognizes the cleaved and processed carboxyterminal octapeptide of VWFpp was used to visualize endogenous VWFpp [19]. Immunoblot analysis confirmed that in both endothelial and platelet lysates this VWFpp antibody exclusively recognizes a 100 kDa protein corresponding to the size of VWFpp (Supplemental Figure 3). Probing for VWF it was clear that platelets, unlike endothelial cells, contain only mature VWF and no detectable proVWF (Supplemental Figure 3), which suggests that proteolytic processing of proVWF into mature VWF and VWFpp is completed before or during the formation of alpha-granules in

megakaryocytes and does not continue post-budding of platelets. Thus, the striking overlap of VWF and VWFpp in our SIM analysis suggests that both proteins are incorporated into the same supramolecular structures within alpha-granules and is not the result of cross-reaction of the VWFpp antibody with unprocessed proVWF.

Differential loss of VWF and VWFpp from post-exocytotic alpha-granules of activated platelets

We next investigated VWF and VWFpp secretion from individual platelet alpha-granules following strong activation of PAR-1 (20 μM PAR-1 ap) or GPVI (1 μg/ml CRP-XL) signaling pathways to drive a high level of platelet activation and degranulation (Supplemental Figure 4 and 5). We quantified the numbers of VWF+ and VWFpp+ structures (alpha-granules) before and after stimulation using 3D-SIM. After PAR-1 stimulation we observed little change in the numbers of VWF+ structures, however, there was a dramatic reduction in VWFpp+ structures consistent with secretion of VWFpp (Figure 2A). The remaining VWF staining was confined to P-selectin (CD62P) labeled structures, suggesting that the protein mostly resides in post-exocytotic alpha-granules (Supplemental Figure 6).Stimulation with 1 μg/ml CRP-XL gave similar results to PAR-1 ap (Figure 2C). These data suggest that VWF and VWFpp, despite their close proximity within alpha-granules in resting platelets, may be differentially released by activated platelets.

As differences in VWF and VWFpp release in relation to agonist responsiveness may be explained by the large differences in size between VWF and VWFpp (VWFpp is a 100 kDa protein, while ultra-large VWF multimers can be in excess of 100 MDa), we also looked at exocytosis of other alpha-granule constituents. SPARC (40 kDa) immunoreactivity was decreased more extensively than for VWF (Figure 3A), however

changes in fibrinogen (~340 kDa) immunoreactivity were qualitatively similar to that of VWF (Figure 3B). This would suggest that additional factors other than protein size play a role in facilitating the differential agonist responsiveness of VWF versus VWFpp.

Differential release of VWF and VWFpp relates to agonist responsiveness

Having established that strong platelet stimulation results in differential release of VWF and VWFpp we next asked whether this phenomenon was influenced by stimulus strength. For this we used a semi-automated quantitative workflow on 3D-SIM images [22] of platelets activated with a broad concentration range of PAR-1 and CRP-XL that partially or fully trigger alpha-granule release (Supplemental Figure 4). We found that differential release of VWF and VWFpp was apparent at all stimulus concentrations of PAR-1 ap (Figure 4A), however, it was clear that less VWFpp was retained in post-exocytosis alpha-granules as the stimulus strength was increased. At 0.625 μM PAR-1 ap the fraction of VWFpp+ alpha-granules was **76.8%,** compared to control platelets (**p<0.0001**, two-way ANOVA), and this fraction reduced to **23.4%** at 20 μM PAR-1 ap (**p<0.0001,** two-way ANOVA). In contrast, for 20 μM PAR-1 ap the fraction of VWF+ alpha-granules were **80.9%** of control (**p<0.0001,** two-way ANOVA). This difference between retention of VWF and VWFpp was significant at all stimulus strengths. Similar findings were obtained using CRP-XL (Supplemental Figure 7A-B). Consistent with our 3D-SIM based exocytosis assay, biochemical analysis showed that VWFpp and VWF are differentially secreted following dose-dependent activation of PAR-1 or GPVI signaling (Figure 4C-D, Supplemental Figure 7C-D).

The release of SPARC and fibrinogen from alpha-granules showed a different pattern (Supplemental Figure 8). The fraction of SPARC+ or fibrinogen+ alpha-granules

present in stimulated platelets reduced to **60.7%** and **67.6%** of control at 20 μM PAR-1 ap. The data illustrates that the extent of cargo release is protein specific.

In conclusion, we observe a large disparity in alpha-granule release of VWF versus VWFpp, where the former is partially retained in alpha-granules, even under strong stimulatory conditions. In contrast, VWFpp release is sensitive to lower agonist concentrations.

Anti-VWF nanobody incorporates in post-exocytotic VWF$^+$ structures in degranulation-dependent manner

Finally, we wanted to study how and when individual alpha-granule structures differentially release VWF versus VWFpp. As we clearly identified granule populations that contained residual VWF, but no more VWFpp, this would suggest that individual alpha-granules could perform a kiss-and-run type of exocytosis that facilitates release of selective alpha-granule cargo. To investigate this further, we performed a platelet degranulation experiment with an anti-VWF nanobody added in suspension, under the assumption that opening of an alpha-granule during exocytosis would facilitate uptake of the nanobody. We found that uptake of the nanobody was directly dependent on the degree of platelet stimulation and thus degranulation, whereas a control R2 nanobody non-specific for VWF did not show any signal by flow cytometry (Supplemental Figure 10A). Additionally, permeabilized platelets showed an increasingly higher mean fluorescent intensity (MFI) at higher doses of PAR-1, suggesting increasing amounts of nanobody specifically inside platelets (Supplemental Figure 10A). We further confirmed this with confocal imaging, where we observed accumulation of the nanobody inside the tubulin-ring at 20 μM PAR-1 ap but not in resting platelets (Supplemental Figure 10B). Additionally, the nanobody co-localized completely with

residual VWF$^+$-structures suggesting that all VWF$^+$ granules are post-exocytotic under these conditions. Together, these findings show that uptake of the VWF nanobody is degranulation dependent. Ultimately, we analyzed individual alpha-granules that were able to take up the VWF nanobody through 3D-SIM. In accordance with the flow cytometry and confocal data, we found an increasing population of VWF nanobody$^+$ structures co-localizing with residual VWF that was directly related to the degree of stimulation. Most resting platelets contained granules with overlapping VWF and VWFpp signal (Figure 5A). At a low dose of PAR-1 ap (Figure 5B), only a minority of granules was strongly positive for the nanobody. The majority of granules however was VWF$^+$ and VWFpp$^+$ but revealed weakly staining for the nanobody. At maximum dose of PAR-1 ap, we found a majority of VWF nanobody$^+$ and VWF$^+$ granules, but these did not contain any VWFpp (Figure 5A-B), suggesting this content has been released during granule opening. Taken together, our findings imply that increasing doses of PAR-1 ap trigger large-scale release of VWFpp from alpha-granules, while VWF is partially retained in such post-exocytotic granules as evidenced by PAR-1 dependent accumulation of VWF nanobody in VWFpp$^-$VWF$^+$ structures. Our cumulative findings show that alpha-granules may exclusively release content like VWFpp while maintaining other cargo, like VWF, under the conditions described in our work.

Discussion

Important biochemical and functional differences exist between platelet and endothelial (plasma) VWF [40] that suggest dissimilarities in biosynthesis of VWF between endothelial cells and megakaryocytes: platelet VWF is composed of higher molecular weight multimers, carries different N-linked glycan structures which makes it more resistant to proteolysis by ADAMTS13 [41] and has higher binding affinity for alphaIIbβ3-integrin [42]. In this study, we investigated storage and exocytosis of VWF and VWFpp from platelet alpha-granules through quantitative super resolution microscopy. Our results show that VWFpp is eccentrically localized within alpha-granules in close proximity to mature VWF. In endothelial cells VWFpp integrates in tubules composed of helically condensed VWF multimers that are found within WPBs. Given that similar tubules, albeit shorter in length, have been observed in platelet alpha-granules [21], we speculate that VWFpp is similarly arranged within VWF tubules as in endothelial WPBs.

In contrast to WPBs, where the tubular arrangement of VWF is essential for rapid and efficient release of VWF upon exocytosis, alpha-granules only release a limited amount of their VWF, even at agonist concentrations that elicit maximum surface exposure of P-selectin and lead to incorporation of anti-VWF nanobody into practically all remaining VWF positive structures. The latter is important because it implies that all these granules have undergone a granule fusion event that generated a fusion pore in contact with the extracellular space. Additionally, we found evidence for differential release of VWFpp and VWF, showing that individual alpha-granules can preferentially release their VWFpp cargo while retaining VWF. Differential release was dependent on stimulus strength but not related to the type of agonist we used in our study.

This is in sharp contrast with the 1:1 stoichiometry between VWF and VWFpp that is released from endothelial cells [16]. What could explain the difference in secretion efficiency between VWF and VWFpp from alpha-granules? Earlier studies on the organization and exocytosis of different types of alpha-granule cargo have resulted in several models as to how platelets are able to (differentially) release their content. Based on localization of a number of alpha-granule cargo proteins, including VWF and fibrinogen as well as several pro- and anti-angiogenic mediators, it was postulated that subpopulations of alpha-granules exist based on inclusion of cargo with opposing functions [31,43]. Preferential mobilization of one of these subpopulations by specific agonists would then lead to differential release of distinct functional classes of alpha-granule cargo, giving platelets the opportunity to direct their secretory response in a context-specific manner. However, this hypothesis was significantly challenged by quantitative, high-resolution imaging that showed that alpha-granule cargo is stochastically packaged in alpha-granules, but segregated within subdomains of the granule matrix [29,32,33]. Kinetic release studies also showed little evidence of specific alpha-granule subpopulations, but instead identified 3 classes of cargo release based on their rate constants (fast, intermediate and slow) in which the alpha-granule cargo distribution is random [28]. Several non-mutually exclusive mechanisms have been proposed that can achieve differential release of VWF and other cargo from the same granule, such as exocytotic fusion mode (direct vs. lingering kiss vs. compound fusion) [44,45] from WPBs, or differences in cargo solubilization, for instance by polar release of non-homogenously distributed cargo from one side of the alpha-granule [28]. The nearly perfect overlap between VWF and VWFpp that we observed in resting platelets (Figure 1-2, S2) suggests both proteins are localized in the same alpha-granules and occupy the same granule subdomains, which rules out that the differences in their

release were reflective of granule subpopulations or could have been the result of polar release of cargo from one end of the granule. Differential release through premature closure of the fusion pore, such as in lingering kiss exocytosis [44], is also unlikely to serve as an explanation since the size of VWFpp (~100 kDa) would require the fusion pore to fully expand before release. Indeed, we did not find an obvious correlation between releasability and size as SPARC (40 kDa) was less sensitive to low concentration stimulation and achieved lower maximal release than VWFpp (Supplemental Figure 8).

In line with previous reports by others [27,46], we frequently observed a clustering of VWF positive structures in the central area of activated platelets that were negative for VWFpp, especially at higher agonist concentrations (Figure 4, Supplemental Figure 7). In some cases, a continuous P-selectin staining enveloping several VWF positive structures (Supplemental Figure 6) was present, reminiscent of several alpha-granules that had engaged in compound fusion. Possibly, this exocytotic fusion mode poses no obstacle for VWFpp but does not favor the release of bulky, multimeric cargo such as VWF, for instance by preventing the orderly unfurling of VWF tubules [45,47]. This may indirectly also relate to differences in solubility of VWF and VWFpp, such as previously observed during loss from the cell surface of endothelial cells following release from WPBs [17]. As a result, VWF remains stuck in post-fusion alpha-granules while VWFpp is efficiently released.

While traces of VWFpp may stick to the D'D3 region of VWF post-release [48], it is likely that after exocytosis its extracellular course is primarily VWF-independent, as attested by the large difference in plasma survival between VWF and VWFpp [49]. However, despite the well-documented pleiotropic roles of VWF, the biological function of extracellular VWFpp is still unclear. Several *in vitro* studies have demonstrated that

bovine VWFpp can bind to collagen type I [50] and that this interaction can block collagen-induced platelet aggregation [51]. VWFpp also contains an RGD sequence, a motif that can serve as a ligand for a subfamily of integrins that contain α5, α8, αv and αIIb subunits. The VWFpp RGD motif is not strongly conserved between species [52], the integrin receptor for this site has not been identified and its significance remains uncertain as the RGD sequence appears to be unfavorably arranged within the native conformation to support adhesive interactions [51]. Bovine VWFpp can bind alpha4β1- and alpha9β1-integrins, which are expressed on lymphocytes, monocytes and neutrophils, via a sequence within the VWD2 domain that is conserved in humans [53–55]. Another ligand for these integrins, coagulation factor FXIII, has been shown to cross link VWFpp to the extracellular matrix protein laminin [55–57]. Possibly, focused release of VWFpp from degranulating platelets during the initial thrombus formation and incorporation in the adhesive surface via laminin and collagen provides a mechanism to influence the adhesive properties of the exposed extracellular matrix and direct hemostatic and immune responses following vascular injury. Recent reports have emerged that VWFpp can contribute to platelet adhesion to collagen surfaces and enhance thrombus mass in a glycan-dependent manner [58], and that in a murine model of deep vein thrombosis VWFpp incorporates in venous thrombi near regions of active thrombus formation [59].

We have recently shown that PF4 levels in plasma are positively correlated with current severity of bleeding phenotype in VWD type 1 patients [60]. PF4 is a chemokine that is mainly produced by megakaryocytes and stored in platelet alpha-granules, which means that systemic PF4 levels are reflective of platelet degranulation. One possible explanation for the observed association with bleeding severity in this group is that apart from a quantitative deficiency of VWF in plasma, the hemostatic contribution of

platelets is impaired by premature release of alpha-granules. This could lead to insufficient delivery of their hemostatic content, such as platelet VWF and other alpha-granule cargo, to sites of vascular injury. A number of studies have focused on the role of platelet derived VWF in hemostasis [61–65]. VWD patients with mild and severe circulating VWF deficiencies who still have residual platelet VWF show a milder clinical phenotype [60,66]. Platelet VWF has also been reported to be important for DDAVP-related amelioration of bleeding times in subgroups of type 1 VWD patients [67]. Together this leads to the notion that release of platelet VWF helps to establish hemostasis in these patients. Our data suggest that following activation the majority of mature VWF actually remains within the platelets, well away from supporting any interactions that can contribute to hemostatic functions of platelets such as adhesion or aggregation. This is in contrast to its proteolytic cleavage product VWFpp, which is efficiently released from platelet alpha-granules following activation and has its own capabilities to interact with components of the extracellular matrix, cellular adhesion receptors and the thrombus. The question thus arises how much of the perceived role of platelet VWF to hemostasis can be attributed to mature VWF and how much (if not more) is actually dependent on VWFpp. More studies that focus on the extracellular role(s) of VWFpp, from endothelial as well as platelet origin, are urgently needed.

Author Contributions

MS, SH, PEB, JAS and RB performed experiments and analyzed data. TC and FWGL provided essential reagents and expertise. MS, SH, AJGJ, JV and RB designed the research and wrote the paper. All authors critically revised and approved of the final version of the manuscript.

Acknowledgements

We thank Dr. Coen Maas (University Medical Center Utrecht, Netherlands) for generous supply of Alpaca anti-VWF CTCK nanobodies. We thank Titus Lemmens (Maastricht University Medical Center+, Netherlands) for stimulating discussion and experimental assistance. This study has been supported by grants from the Landsteiner Stichting voor Bloedtransfusie Research (LSBR-1707 and LSBR-2005) and an EHA Clinical Research Fellowship (A.J.G. Jansen).

Conflict of Interest

F.W.G. Leebeek received research support from CSL Behring, Takeda, uniQure and Sobi and is consultant for uniQure, Biomarin, CSL Behring and Takeda, of which the fees go to the institute. He was a DSMB member for a study sponsored by Roche. A.J.G. Jansen received speaker fees and travel cost payments from 3SBio, Amgen and Novartis, is on the international advisory board at Novartis and received research support from CSL Behring, Principia and Argenx. None of the other authors have conflicts of interest to declare.

References

1 Yadav S, Storrie B. The cellular basis of platelet secretion: Emerging structure/function relationships. *Platelets* 2017; **28**: 108–18.

2 Karampini E, Bierings R, Voorberg J. Orchestration of Primary Hemostasis by Platelet and Endothelial Lysosome-Related Organelles. *Arterioscler, Thromb Vasc Biol* 2020; **40**: 1441–53.

3 Springer TA. Von Willebrand factor, Jedi knight of the bloodstream. *Blood* 2014; **124**: 1412–25.

4 Schillemans M, Karampini E, Kat M, Bierings R. Exocytosis of Weibel–Palade bodies: how to unpack a vascular emergency kit. *J Thromb Haemost* 2019; **17**: 6–18.

5 Valentijn KM, Sadler JE, Valentijn JA, Voorberg J, Eikenboom J. Functional architecture of Weibel-Palade bodies. *Blood* 2011; **117**: 5033–43.

6 Vischer UM, Wagner DD. von Willebrand factor proteolytic processing and multimerization precede the formation of Weibel-Palade bodies. *Blood* 1994; **83**: 3536–44.

7 Zeng J, Shu Z, Liang Q, Zhang J, Wu W, Wang X, Zhou A. Structural basis of von Willebrand factor multimerization and tubular storage. *Blood* 2022; **139**: 3314–24.

8 Anderson JR, Li J, Springer TA, Brown A. Structures of VWF tubules before and after concatemerization reveal a mechanism of disulfide bond exchange. *Blood* 2022; **140**: 1419–30.

9 Wagner DD, Saffaripour S, Bonfanti R, Sadler JE, Cramer EM, Chapman B,

Mayadas TN. Induction of specific storage organelles by von Willebrand factor propolypeptide. *Cell* 1991; **64**: 403–13.

10 Voorberg J, Fontijn R, Calafat J, Janssen H, Van Mourik JA, Pannekoek H. Biogenesis of von Willebrand factor-containing organelles in heterologous transfected CV-1 cells. *EMBO J* 1993; **12**: 749–58.

11 Haberichter SL, Fahs SA, Montgomery RR. Von Willebrand factor storage and multimerization: 2 independent intracellular processes. *Blood* 2000; **96**: 1808–15.

12 Huang RH, Wang Y, Roth R, Yu X, Purvis AR, Heuser JE, Egelman EH, Sadler JE. Assembly of Weibel-Palade body-like tubules from N-terminal domains of von Willebrand factor. *Proc Natl Acad Sci U S A* 2008; **105**: 482–7.

13 Berriman JA, Li S, Hewlett LJ, Wasilewski S, Kiskin FN, Carter T, Hannah MJ, Rosenthal PB. Structural organization of Weibel-Palade bodies revealed by cryo-EM of vitrified endothelial cells. *Proc Natl Acad Sci U S A* 2009; **106**: 17407–12.

14 Michaux G, Abbitt KB, Collinson LM, Haberichter SL, Norman KE, Cutler DF. The physiological function of von Willebrand's factor depends on its tubular storage in endothelial Weibel-Palade bodies. *Dev Cell* 2006; **10**: 223–32.

15 Conte IL, Cookson E, Hellen N, Bierings R, Mashanov G, Carter T. Is there more than one way to unpack a Weibel-Palade body? *Blood*. 2015. p. 2165–7.

16 Wagner DD, Fay PJ, Sporn LA, Sinha S, Lawrence SO, Marder VJ. Divergent fates of von Willebrand factor and its propolypeptide (von Willebrand antigen II) after secretion from endothelial cells. *Proc Natl Acad Sci U S A* 1987; **84**:

1955–9.

17 Hannah MJ, Skehel P, Erent M, Knipe L, Ogden D, Carter T. Differential kinetics of cell surface loss of von Willebrand factor and its propolypeptide after secretion from Weibel-Palade bodies in living human endothelial cells. *J Biol Chem* 2005; **280**: 22827–30.

18 Babich V, Knipe L, Hewlett L, Meli A, Dempster J, Hannah MJ, Carter T. Differential effect of extracellular acidosis on the release and dispersal of soluble and membrane proteins secreted from the Weibel-Palade body. *J Biol Chem* 2009; **284**: 12459–68.

19 Hewlett L, Zupančič G, Mashanov G, Knipe L, Ogden D, Hannah MJ, Carter T. Temperature-dependence of weibel-palade body exocytosis and cell surface dispersal of von willebrand factor and its propolypeptide. *PLoS One* 2011; **6**: e27314.

20 Cramer E, Meyer D, le Menn R, Breton-Gorius J. Eccentric localization of von Willebrand factor in an internal structure of platelet alpha-granule resembling that of Weibel-Palade bodies. *Blood* 1985; **66**: 710–3.

21 Van Nispen Tot Pannerden H, De Haas F, Geerts W, Posthuma G, Van Dijk S, Heijnen HFG. The platelet interior revisited: Electron tomography reveals tubular α-granule subtypes. *Blood* 2010; **116**: 1147–56.

22 Swinkels M, Atiq F, Bürgisser PE, Slotman JA, Houtsmuller AB, de Heus C, Klumperman J, Leebeek FWG, Voorberg J, Jansen AJG, Bierings R. Quantitative 3D microscopy highlights altered von Willebrand factor α-granule storage in patients with von Willebrand disease with distinct pathogenic

mechanisms. *Res Pract Thromb Haemost* Wiley-Blackwell; 2021; **5**.

23 Koutts J, Walsh PN, Plow EF, Fenton IInd JW, Bouma BN, Zimmerman TS. Active release of human platelet factor VIII related antigen by adenosine diphosphate, collagen, and thrombin. *J Clin Invest* J Clin Invest; 1978; **62**: 1255–63.

24 Montgomery RR, Zimmerman TS. Von Willebrand's disease antigen II. A new plasma and platelet antigen deficient in severe von Willebrand's disease. *J Clin Invest* 1978; **61**: 1498–507.

25 Scott JP, Montgomery RR. Platelet von Willebrand's antigen II: Active release by aggregating agents and a marker of platelet release reaction in vivo. *Blood* 1981; **58**: 1075–80.

26 Morgenstern E, Neumann K, Patscheke H. The exocytosis of human blood platelets. A fast freezing and freeze-substitution analysis. *Eur J Cell Biol* 1987; **43**: 273–82.

27 Eckly A, Rinckel JY, Proamer F, Ulas N, Joshi S, Whiteheart SW, Gachet C. Respective contributions of single and compound granule fusion to secretion by activated platelets. *Blood* 2016; **128**: 2538–49.

28 Jonnalagadda D, Izu LT, Whiteheart SW. Platelet secretion is kinetically heterogeneous in an agonist-responsive manner. *Blood* American Society of Hematology; 2012; **120**: 5209–16.

29 Sehgal S, Storrie B. Evidence that differential packaging of the major platelet granule proteins von Willebrand factor and fibrinogen can support their differential release. *J Thromb Haemost* 2007; **5**: 2009–16.

30 Wijten P, Van Holten T, Woo LL, Bleijerveld OB, Roest M, Heck AJR, Scholten A. High precision platelet releasate definition by quantitative reversed protein profiling-brief report. *Arterioscler Thromb Vasc Biol* 2013; **33**: 1635–8.

31 Italiano JE, Richardson JL, Patel-Hett S, Battinelli E, Zaslavsky A, Short S, Ryeom S, Folkman J, Klement GL. Angiogenesis is regulated by a novel mechanism: Pro- and antiangiogenic proteins are organized into separate platelet α granules and differentially released. *Blood* 2008; **111**: 1227–33.

32 Kamykowski J, Carlton P, Sehgal S, Storrie B. Quantitative immunofluorescence mapping reveals little functional coclustering of proteins within platelet α-granules. *Blood* 2011; **118**: 1370–3.

33 Pokrovskaya ID, Yadav S, Rao A, McBride E, Kamykowski JA, Zhang G, Aronova MA, Leapman RD, Storrie B. 3D ultrastructural analysis of α-granule, dense granule, mitochondria, and canalicular system arrangement in resting human platelets. Senis Y, editor. *Res Pract Thromb Haemost* 2020; **4**: 72–85.

34 de Maat S, Clark CC, Barendrecht AD, Smits S, van Kleef ND, El Otmani H, Waning M, van Moorsel M, Szardenings M, Delaroque N, Vercruysse K, Urbanus RT, Sebastian S, Lenting PJ, Hagemeyer C, Renné T, Vanhoorelbeke K, Tersteeg C, Maas C. Microlyse: a thrombolytic agent that targets VWF for clearance of microvascular thrombosis. *Blood* 2022; **139**: 597–607.

35 Costes S V., Daelemans D, Cho EH, Dobbin Z, Pavlakis G, Lockett S. Automatic and quantitative measurement of protein-protein colocalization in live cells. *Biophys J* The Biophysical Society; 2004; **86**: 3993–4003.

36 Bolte S, Cordelières FP. A guided tour into subcellular colocalization analysis in

light microscopy. *Journal of Microscopy*. J Microsc; 2006. p. 213–32.

37 Karampini E, Bürgisser PE, Olins J, Mulder AA, Jost CR, Geerts D, Voorberg J, Bierings R. Sec22b determines Weibel-Palade body length by controlling anterograde endoplasmic reticulum-Golgi transport. *Haematologica* Ferrata Storti Foundation; 2021; **106**: 1138–47.

38 Schillemans M, Karampini E, Van Den Eshof BL, Gangaev A, Hofman M, Van Breevoort D, Meems H, Janssen H, Mulder AA, Jost CR, Escher JC, Adam R, Carter T, Koster AJ, Van Den Biggelaar M, Voorberg J, Bierings R. Weibel-palade body localized syntaxin-3 modulates von willebrand factor secretion from endothelial cells. *Arterioscler Thromb Vasc Biol* 2018; **38**: 1549–61.

39 Van Den Biggelaar M, Bierings R, Storm G, Voorberg J, Mertens K. Requirements for cellular co-trafficking of factor VIII and von Willebrand factor to Weibel-Palade bodies. *J Thromb Haemost* 2007; **5**: 2235–43.

40 McGrath RT, McRae E, Smith OP, O'Donnell JS. Platelet von Willebrand factor - Structure, function and biological importance. *British Journal of Haematology*. 2010. p. 834–43.

41 McGrath RT, Van Den Biggelaar M, Byrne B, O'Sullivan JM, Rawley O, O'Kennedy R, Voorberg J, Preston RJS, O'Donnell JS. Altered glycosylation of platelet-derived von Willebrand factor confers resistance to ADAMTS13 proteolysis. *Blood* 2013; **122**: 4107–10.

42 Williams SB, McKeown LP, Krutzsch H, Hansmann K, Gralnick HR. Purification and characterization of human platelet von Willebrand factor. *Br J Haematol* 1994; **88**: 582–91.

43 Battinelli EM, Thon JN, Okazaki R, Peters CG, Vijey P, Wilkie AR, Noetzli LJ, Flaumenhaft R, Italiano JE. Megakaryocytes package contents into separate a-granules that are differentially distributed in platelets. *Blood Adv* American Society of Hematology; 2019; **3**: 3092–8.

44 Babich V, Meli A, Knipe L, Dempster JE, Skehel P, Hannah MJ, Carter T. Selective release of molecules from Weibel-Palade bodies during a lingering kiss. *Blood* American Society of Hematology; 2008; **111**: 5282–90.

45 Stevenson NL, White IJ, McCormack JJ, Robinson C, Cutler DF, Nightingale TD. Clathrin-mediated post-fusion membrane retrieval influences the exocytic mode of endothelial Weibel-Palade bodies. *J Cell Sci* 2017; **130**: 2591–605.

46 Stenberg PE, Shuman MA, Levine SP, Bainton DF. Redistribution of alpha-granules and their contents in thrombin-stimulated platelets. *J Cell Biol* 1984; **98**: 748–60.

47 Mourik MJ, Valentijn JA, Voorberg J, Koster AJ, Valentijn KM, Eikenboom J. Von Willebrand factor remodeling during exocytosis from vascular endothelial cells. *J Thromb Haemost* 2013; **11**: 2009–19.

48 Madabhushi SR, Shang C, Dayananda KM, Rittenhouse-Olson K, Murphy M, Ryan TE, Montgomery RR, Neelamegham S. Von Willebrand factor (VWF) propeptide binding to VWF D'D3 domain attenuates platelet activation and adhesion. *Blood* Â© 2012 by The American Society of Hematology; 2012; **119**: 4769–78.

49 Van Mourik JA, Boertjes R, Huisveld IA, Fijnvandraat K, Pajkrt D, Van Genderen PJJ, Fijnheer R. von Willebrand factor propeptide in vascular

disorders: A tool to distinguish between acute and chronic endothelial cell perturbation. *Blood* 1999; **94**: 179–85.

50 Takagi J, Kasahara K, Sekiya F, Inada Y, Saito Y. A collagen-binding glycoprotein from bovine platelets is identical to propolypeptide of von Willebrand factor. *J Biol Chem* 1989; **264**: 10425–30.

51 Takagi J, Sekiya F, Kasahara K, Inada Y, Saito Y. Inhibition of platelet-collagen interaction by propolypeptide of von Willebrand factor. *J Biol Chem* 1989; **264**: 6017–20.

52 Janel N, Ribba AS, Chérel G, Kerbiriou-Nabias D, Meyer D. Primary structure of the propeptide and factor VIII-binding domain of bovine von Willebrand factor. *Biochim Biophys Acta - Protein Struct Mol Enzymol* 1997; **1339**: 4–8.

53 Takagi J, Sudo Y, Saito T, Saito Y. β1-integrin-mediated adhesion of melanoma cells to the propolypeptide of von Willebrand factor. *Eur J Biochem* Eur J Biochem; 1994; **222**: 861–8.

54 Isobe T, Hisaoka T, Shimizu A, Okuno M, Aimoto S, Takada Y, Saito Y, Takagi J. Propolypeptide of von Willebrand factor is a novel ligand for very late antigen-4 integrin. *J Biol Chem* 1997; **272**: 8447–53.

55 Takahashi H, Isobe T, Horibe S, Takagi J, Yokosaki Y, Sheppardi D, Saito Y. Tissue transglutaminase, coagulation factor XIII, and the pro-polypeptide of von Willebrand factor are all ligands for the integrins α9β1 and α4β1. *J Biol Chem* 2000; **275**: 23589–95.

56 Usui T, Takagi J, Saito Y. Propolypeptide of von Willebrand factor serves as a substrate for Factor XIIIa and is cross-linked to laminin. *J Biol Chem* 1993; **268**:

12311–6.

57 Takagi J, Aoyama T, Ueki S, Ohba H, Saito Y, Lorand L. Identification of Factor-XIIIa-Reactive Glutaminyl Residues in the Propolypeptide of Bovine von Willebrand Factor. *Eur J Biochem* 1995; **232**: 773–7.

58 Rawley O, Lillicrap D. Functional Roles of the von Willebrand Factor Propeptide. *Hamostaseologie* 2021; **41**: 063–8.

59 Rawley O, Dwyer C, Nesbitt K, Notley C, Michels A, Lillicrap D. The VWF Propeptide Is A Novel Component Of Venous Thrombi In A Mouse Model Of DVT [Abstract PB0802]. *Res Pract Thromb Haemost* 2022; **6**.

60 Swinkels M, Atiq F, Bürgisser PE, van Moort I, Meijer K, Eikenboom J, Fijnvandraat K, van Galen KPM, de Meris J, Schols SEM, van der Bom JG, Cnossen MH, Voorberg J, Leebeek FWG, Bierings R, Jansen AJG, Fijnvandraat K, Coppens M, de Meris J, Nieuwenhuizen L, et al. Platelet degranulation and bleeding phenotype in a large cohort of Von Willebrand disease patients. *Br J Haematol* 2022; **197**: 497–501.

61 Gralnick H, Rick M, McKeown L, Williams S, Parker R, Maisonneuve P, Jenneau C, Sultan Y. Platelet von Willebrand factor: an important determinant of the bleeding time in type I von Willebrand's disease. *Blood* 1986; **68**: 58–61.

62 Fressinaud E, Baruch D, Rothschild C, Baumgartner H, Meyer D. Platelet von Willebrand factor: evidence for its involvement in platelet adhesion to collagen. *Blood* American Society of Hematology; 1987; **70**: 1214–7.

63 Rodeghiero F, Castaman G, Ruggeri M, Tosetto A. The bleeding time in normal subjects is mainly determined by platelet von Willebrand factor and is

independent from blood group. *Thromb Res* 1992; **65**: 605–15.

64 Kanaji S, Fahs SA, Shi Q, Haberichter SL, Montgomery RR. Contribution of platelet vs. endothelial VWF to platelet adhesion and hemostasis. *J Thromb Haemost* 2012; **10**: 1646–52.

65 Verhenne S, Denorme F, Libbrecht S, Vandenbulcke A, Pareyn I, Deckmyn H, Lambrecht A, Nieswandt B, Kleinschnitz C, Vanhoorelbeke K, De Meyer SF. Platelet-derived VWF is not essential for normal thrombosis and hemostasis but fosters ischemic stroke injury in mice. *Blood* 2015; **126**: 1715–22.

66 Bowman ML, Pluthero FG, Tuttle A, Casey L, Li L, Christensen H, Robinson KS, Lillicrap D, Kahr WHA, James P. Discrepant platelet and plasma von Willebrand factor in von Willebrand disease patients with p.Pro2808Leufs*24. *J Thromb Haemost* 2017; **15**: 1403–11.

67 Mannucci PM, Lombardi R, Bader R, Vianello L, Federici AB, Solinas S, Mazzucconi MG, Mariani G. Heterogeneity of type I von Willebrand disease: Evidence for a subgroup with an abnormal von Willebrand factor. *Blood* American Society of Hematology; 1985; **66**: 796–802.

Figure Legends

Figure 1: VWF and VWFpp localization in resting platelets. (A,B) Resting platelets were stained for alpha-tubulin (magenta), VWF (red, mouse monoclonal anti-VWF (CLB-RAg20)) and (A) VWFpp (green) or (B) Fibrinogen (green). (C) Resting platelet stained for alpha-tubulin (magenta), VWF (red, rabbit polyclonal anti-VWF (DAKO)) and SPARC (green). Imaging was done by SIM and representative high-resolution single plane zoom-in images are shown, with areas within yellow squares that contain single granules shown magnified on the right (yellow square). Scale bar represents 1 µm. (D-E) Colocalization analysis for VWF with alpha-granule proteins VWFpp, SPARC and Fibrinogen. (D) Pearson's Colocalization Coefficients (PCC) and (E) pairwise Mander's Colocalization Coefficients (MCC) for individual platelet images (VWF-VWFpp n=239, VWF-SPARC n=199, VWF-Fibrinogen n=73) show VWF has higher overlap with VWFpp than with SPARC or Fibrinogen. Bars show means and 95% confidence intervals, mean PCC and MCC values shown in top of graph.

Figure 2: Release of VWF and VWFpp from alpha-granules. Platelets were stimulated for 30 minutes with vehicle or 20 µM PAR-1 ap (A-B) or 1 µg/ml CRP-XL (C) and stained for alpha-tubulin (magenta), VWF (red, CLB-RAg20) and VWFpp (green). Single plane zoom-in images are shown (A,C) as well as a panel of single plane zoom-in images of 10 random platelets (B). Scale bar represents 1 µm.

Figure 3: Release of SPARC and fibrinogen from alpha-granules. Platelets were stimulated with 20 µM PAR-1 and compared to resting platelets for release of alpha-granule proteins. Immunofluorescent staining for alpha-tubulin (magenta) in combination with (A) VWF (red, DAKO) and SPARC (green) or (B) VWF (red, CLB-

RAg20) and Fibrinogen (green). Single plane, representative zoom-in images are shown. Scale bars represent 1 µm.

Figure 4: Dose-response release of VWF and VWFpp. (A) Platelets were stimulated with 0-20 µM PAR-1 ap and stained for alpha-tubulin (magenta), VWF (red, CLB-RAg20) and VWFpp (green). Representative single plane zoom-in images are shown. Scale bars represent 1 µm. (B) VWF and VWFpp release were assessed by quantification of residual VWF+ / VWFpp+ structures in platelets normalized to resting platelets. Counts are pooled from 3 independent healthy donors, 0 µM PAR-1 ap n=435, 0.625 µM PAR-1 ap n=365, 2.5 µM PAR-1 ap n=318, 20 µM PAR-1 ap n=280 platelets. Absolute platelet counts per donor are stated in Supplemental Figure 9. The release (C) and retention (D) of VWF and VWFpp in PAR-1 ap stimulated platelets was measured by ELISA and normalized to resting intracellular content. Statistical analysis by two-way ANOVA with Sidak multiple comparisons test and significance levels of *** = $p<0.001$, **** = $p<0.0001$. Bars show means with 95% confidence intervals.

Figure 5: SIM analysis of VWF nanobody uptake during alpha-granule release. Platelets were stimulated with 0-20 µM of PAR-1 ap in the presence of 1 µg/ml VWF nanobody (magenta) and stained for VWF (red, CLB-RAg20) and VWFpp (green) (A). Single plane, representative zoom-in image of granule content of a resting and maximum stimulated platelet. Magnified region shows single granule content. Scale bar represents 1 µm. (B) Granule populations of VWF/VWFpp/VWF-nanobody positivity were quantified for each stimulus condition. Platelet counts are pooled from 4 independent healthy donors, 0 µM PAR-1 ap n=835, 0.625 µM PAR-1 ap n=696, 2.5 µM PAR-1 ap n=748, 20 µM PAR-1 ap n=620 platelets. Granule counts were normalized to the number of platelets that were analyzed and are indicated within their respective boxes within the stacked bar graph.

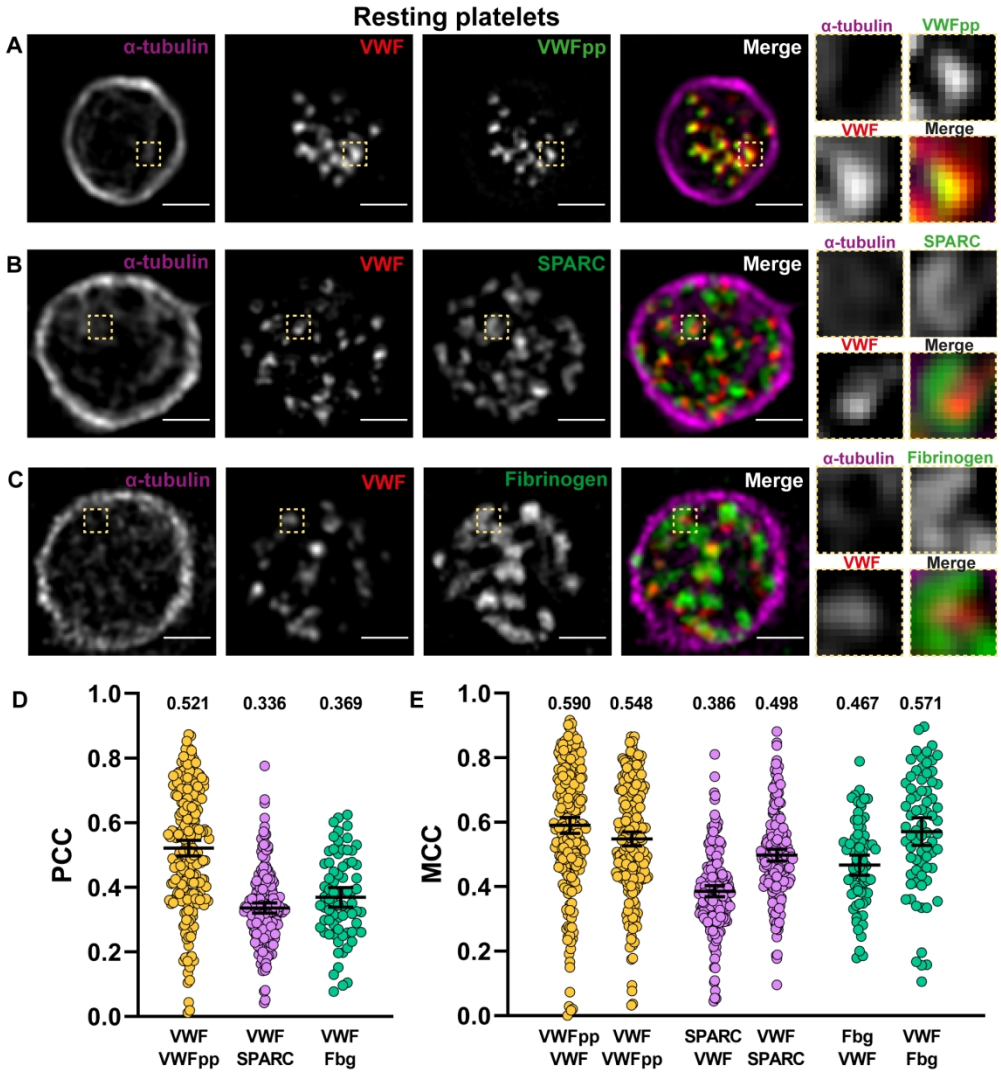

Figure 1: VWF and VWFpp localization in resting platelets. (A,B) Resting platelets were stained for alpha-tubulin (magenta), VWF (red, mouse monoclonal anti-VWF (CLB-RAg20)) and (A) VWFpp (green) or (B) Fibrinogen (green). (C) Resting platelet stained for alpha-tubulin (magenta), VWF (red, rabbit polyclonal anti-VWF (DAKO)) and SPARC (green). Imaging was done by SIM and representative high-resolution single plane zoom-in images are shown, with areas within yellow squares that contain single granules shown magnified on the right (yellow square). Scale bar represents 1 µm. (D-E) Colocalization analysis for VWF with alpha-granule proteins VWFpp, SPARC and Fibrinogen. (D) Pearson's Colocalization Coefficients (PCC) and (E) pairwise Mander's Colocalization Coefficients (MCC) for individual platelet images (VWF-VWFpp n=239, VWF-SPARC n=199, VWF-Fibrinogen n=73) show VWF has higher overlap with VWFpp than with SPARC or Fibrinogen. Bars show means and 95% confidence intervals, mean PCC and MCC values shown in top of graph.

173x188mm (300 x 300 DPI)

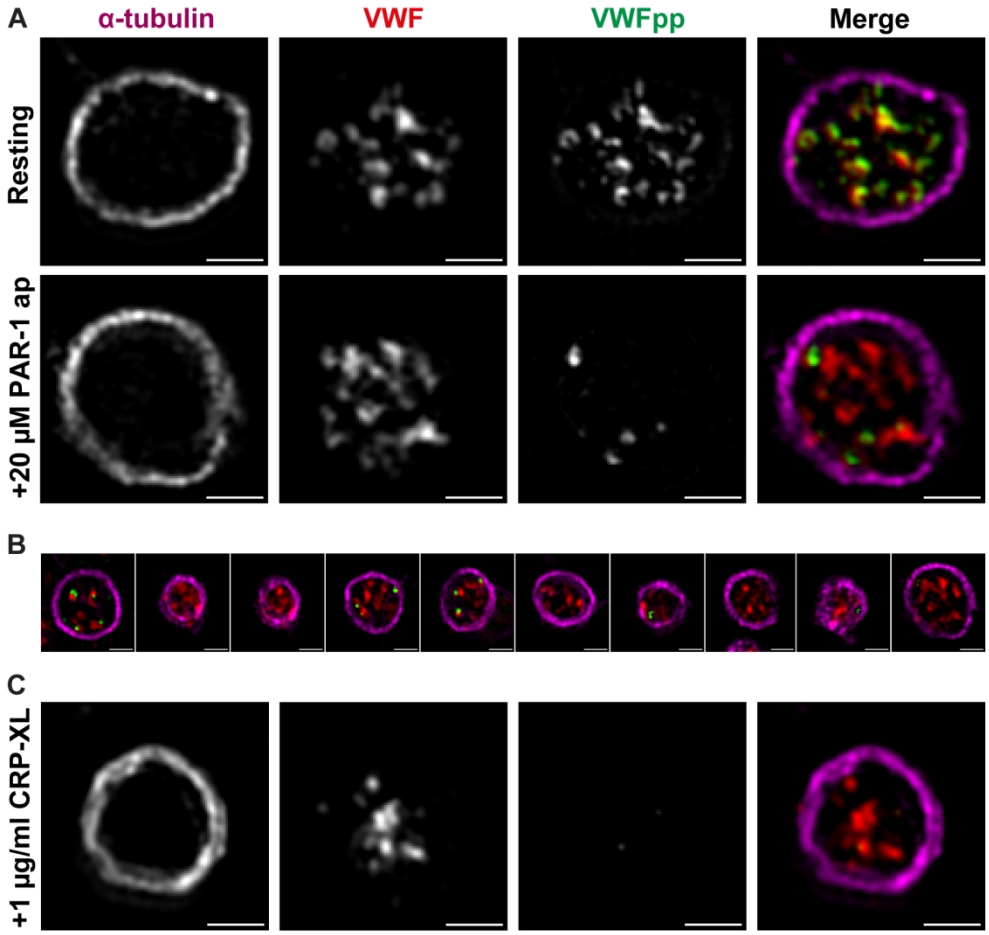

Figure 2: Release of VWF and VWFpp from alpha-granules. Platelets were stimulated for 30 minutes with vehicle or 20 µM PAR-1 ap (A-B) or 1 µg/ml CRP-XL (C) and stained for alpha-tubulin (magenta), VWF (red, CLB-RAg20) and VWFpp (green). Single plane zoom-in images are shown (A,C) as well as a panel of single plane zoom-in images of 10 random platelets (B). Scale bar represents 1 µm.

173x163mm (300 x 300 DPI)

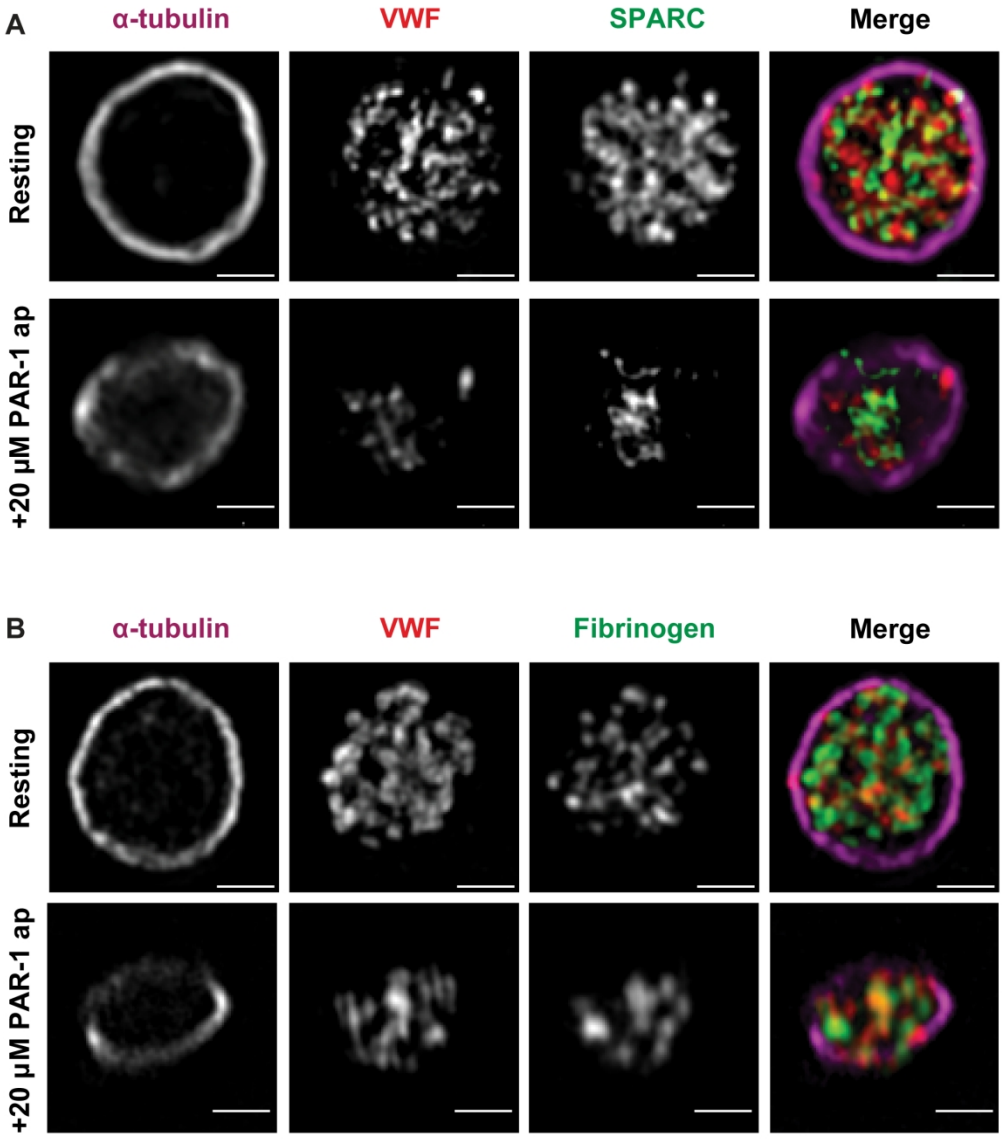

Figure 3: Release of SPARC and fibrinogen from alpha-granules. Platelets were stimulated with 20 µM PAR-1 and compared to resting platelets for release of alpha-granule proteins. Immunofluorescent staining for alpha-tubulin (magenta) in combination with (A) VWF (red, DAKO) and SPARC (green) or (B) VWF (red, CLB-RAg20) and Fibrinogen (green). Single plane, representative zoom-in images are shown. Scale bars represent 1 µm.

173x199mm (300 x 300 DPI)

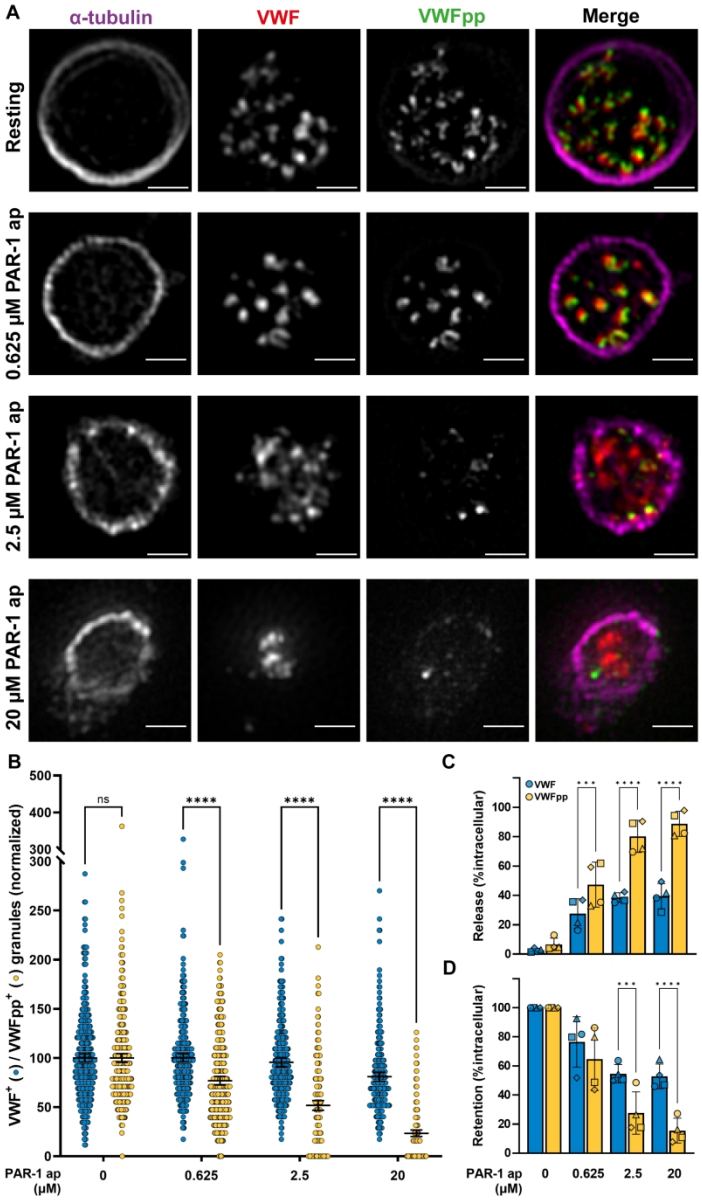

Figure 4: Dose-response release of VWF and VWFpp. (A) Platelets were stimulated with 0-20 µM PAR-1 ap and stained for alpha-tubulin (magenta), VWF (red, CLB-RAg20) and VWFpp (green). Representative single plane zoom-in images are shown. Scale bars represent 1 µm. (B) VWF and VWFpp release were assessed by quantification of residual VWF+ / VWFpp+ structures in platelets normalized to resting platelets. Counts are pooled from 3 independent healthy donors, 0 µM PAR-1 ap n=435, 0.625 µM PAR-1 ap n=365, 2.5 µM PAR-1 ap n=318, 20 µM PAR-1 ap n=280 platelets. Absolute platelet counts per donor are stated in Supplemental Figure 9. The release (C) and retention (D) of VWF and VWFpp in PAR-1 ap stimulated platelets was measured by ELISA and normalized to resting intracellular content. Statistical analysis by two-way ANOVA with Sidak multiple comparisons test and significance levels of *** = p<0.001, **** = p<0.0001. Bars show means with 95% confidence intervals.

173x294mm (300 x 300 DPI)

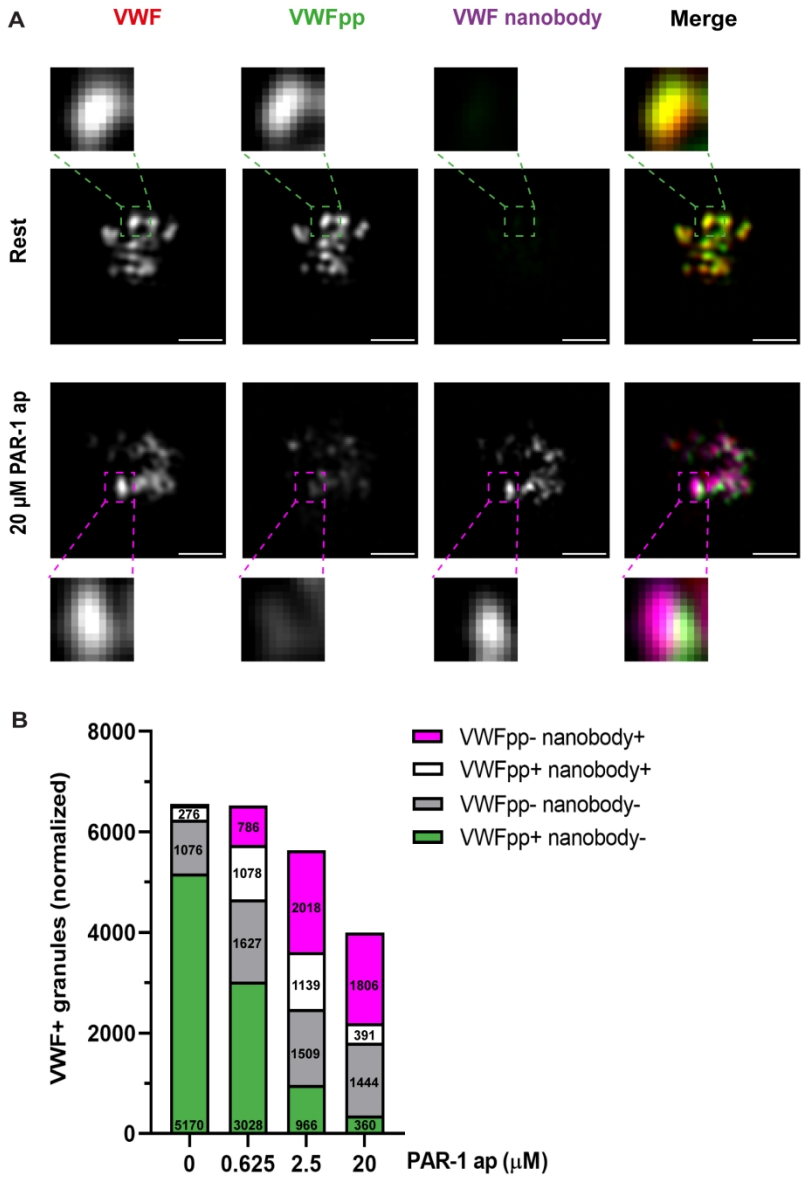

Figure 5: SIM analysis of VWF nanobody uptake during alpha-granule release. Platelets were stimulated with 0-20 µM of PAR-1 ap in the presence of 1 µg/ml VWF nanobody (magenta) and stained for VWF (red, CLB-RAg20) and VWFpp (green) (A). Single plane, representative zoom-in image of granule content of a resting and maximum stimulated platelet. Magnified region shows single granule content. Scale bar represents 1 µm. (B) Granule populations of VWF/VWFpp/VWF-nanobody positivity were quantified for each stimulus condition. Platelet counts are pooled from 4 independent healthy donors, 0 µM PAR-1 ap n=835, 0.625 µM PAR-1 ap n=696, 2.5 µM PAR-1 ap n=748, 20 µM PAR-1 ap n=620 platelets. Granule counts were normalized to the number of platelets that were analyzed and are indicated within their respective boxes within the stacked bar graph.

173x259mm (300 x 300 DPI)

Supplementary information

Supplementary Table S1: Antibodies used in immunofluorescent staining

Antigen	Species (Isotype)	Label	Supplier	Cat. Nr.	Dilution
Von Willebrand factor propeptide	Rabbit	-	Prof. Tom Carter, SGUL	-	1:500
Von Willebrand factor	Rabbit	-	DAKO	A0082	1:500
Von Willebrand factor	Mouse (IgG_{2b})	-	Sanquin	CLB-RAg20	1:500
Alpha-tubulin	Mouse (IgG_{2b})	-	Abcam	ab56676	1:500
Alpha-tubulin	Mouse (IgG_1)	-	Sigma	DM1A	1:500
SPARC	Mouse (IgG_1)	-	SantaCruz	sc-73472	1:500
Fibrinogen	Rabbit	-	DAKO	A0080	1:500
CD62P	Mouse (IgG_1)	-	Bio-Rad	MCA796	1:500
Mouse IgG_1	Goat	CF488A	Biotium	20246	1:1000
Mouse IgG_1	Goat	CF568	Biotium	20248	1:1000
Mouse IgG_1	Goat	CF647	Biotium	20252	1:1000
Mouse IgG_{2b}	Goat	CF647	Biotium	20272	1:1000
Rabbit IgG (H+L)	Goat	CF488	Biotium	20012	1:1000
Rabbit IgG (H+L)	Donkey	AF 568	ThermoFisher	A11042	1:400
Alpaca IgG	Goat	AF 488	Jackson ImmunoResearch	128-545-230	1:400

Supplemental Figure 1

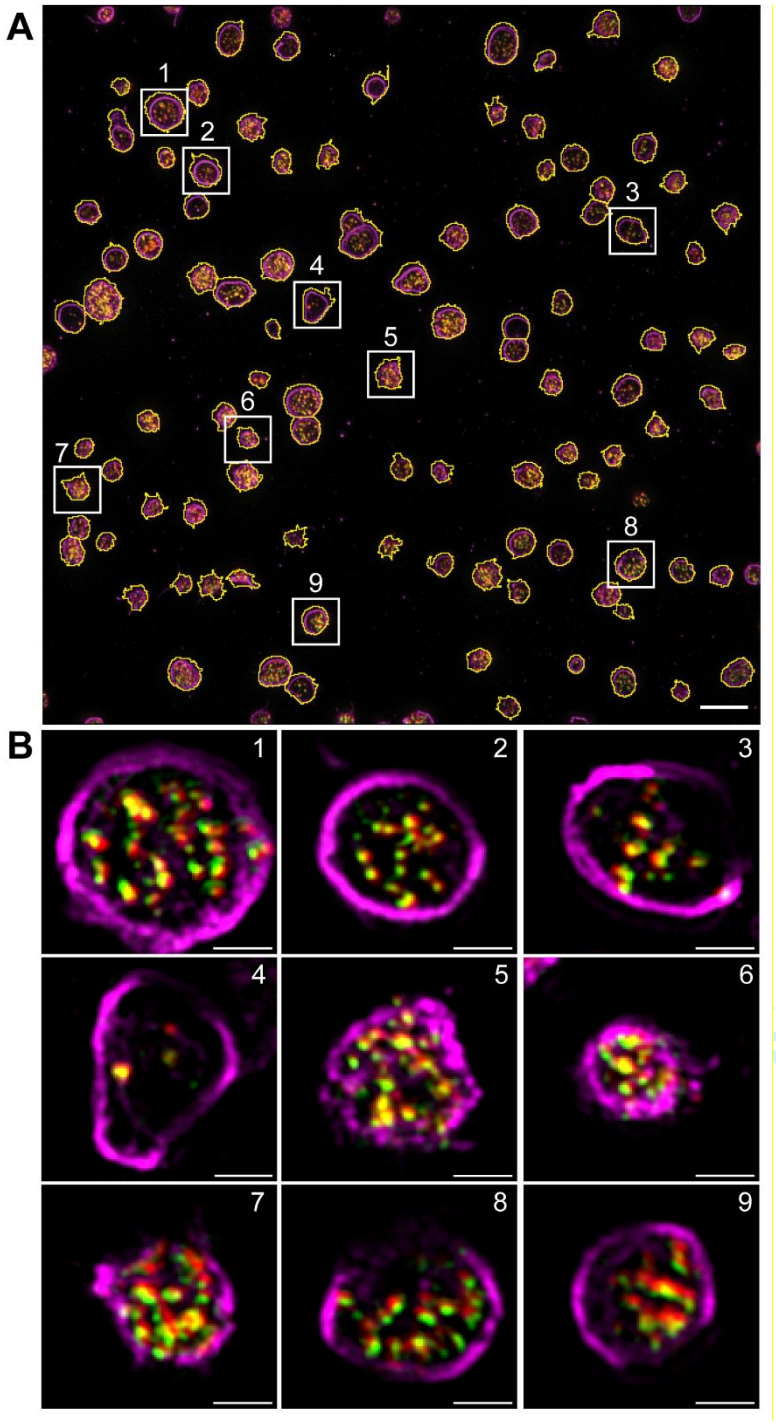

Supplemental Figure 1: VWF and VWFpp localization in resting platelets. Full field of view of resting platelets segmented based on alpha-tubulin staining (magenta) and stained for VWF (red) and VWFpp (green) (A). Highlighted platelets are randomly

selected and presented as single plane zoom-in images in (B). Scale bar represents 5 μM in (A) and 1 μM in (B).

Supplemental Figure 2

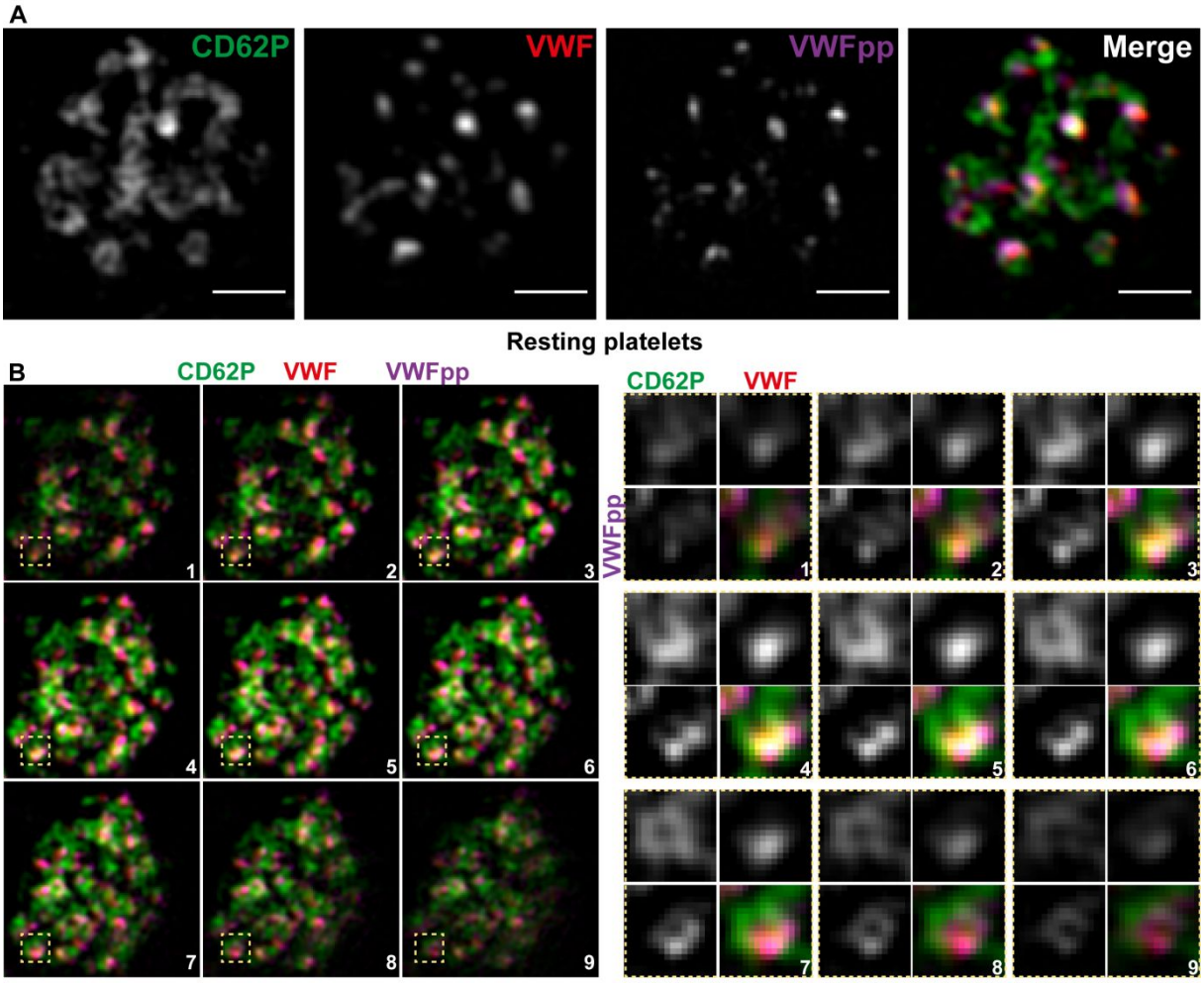

Supplemental Figure 2: 3D VWF and VWFpp localization in CD62P-defined alpha-granular structures. Resting platelets were stained for CD62P (green), VWF (red, CLB-RAg20) and VWFpp (magenta). Representative platelets are shown as single plane zoom-in image (A) or in serial planes of a zoom-in image (B) to illustrate 3D localization of the stained proteins. Single granule details of CD62P/VWF/VWFpp (yellow squares) are shown. Scale bar represents 1 µm.

Supplemental Figure 3

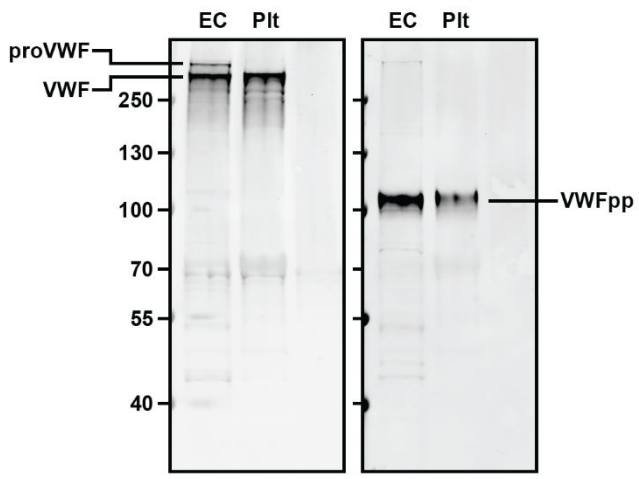

Supplemental Figure 3: VWF and VWFpp immunoblots of endothelial- and platelet lysates. Endothelial and platelet lysates were separated on a 4-12% Bis-Tris gel and probed for VWF (left, DAKO) or VWFpp (right). Bands corresponding to proVWF, mature VWF (VWF) and VWFpp are indicated.

Supplemental Figure 4

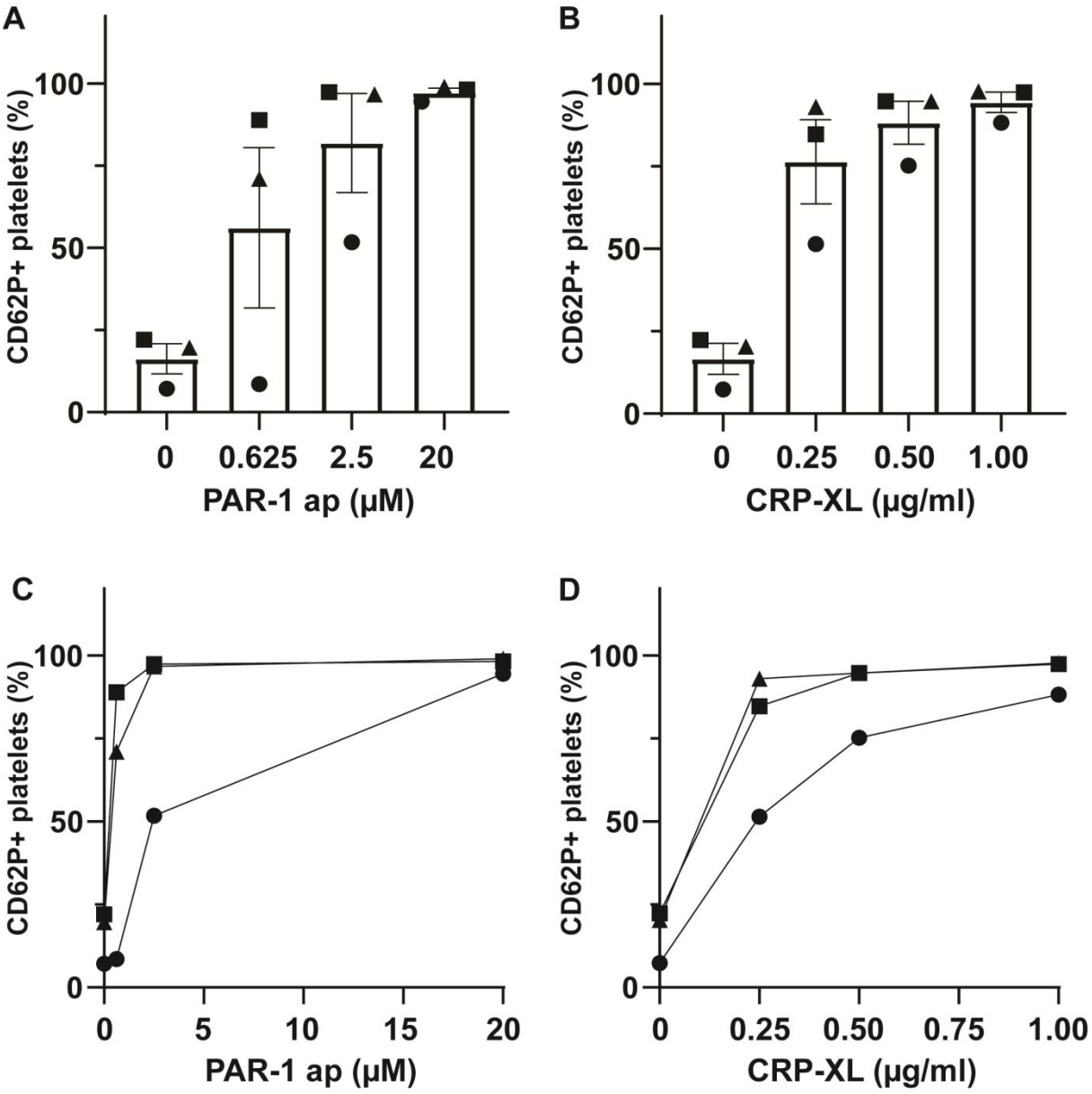

Supplemental Figure 4: Alpha-granule release assessed by FACS analysis of P-selectin exposure. Platelets were stimulated with increasing doses of PAR-1 ap (A) or CRP-XL (B) and quantified for CD62P+ cell surface exposure by flow cytometry. Symbols represent individual donors (n=3). Individual dose response curves are shown in C (PAR-1 ap) and D (CRP-XL) with symbols representing unique donors. Data presented as mean ± SD.

Supplemental Figure 5

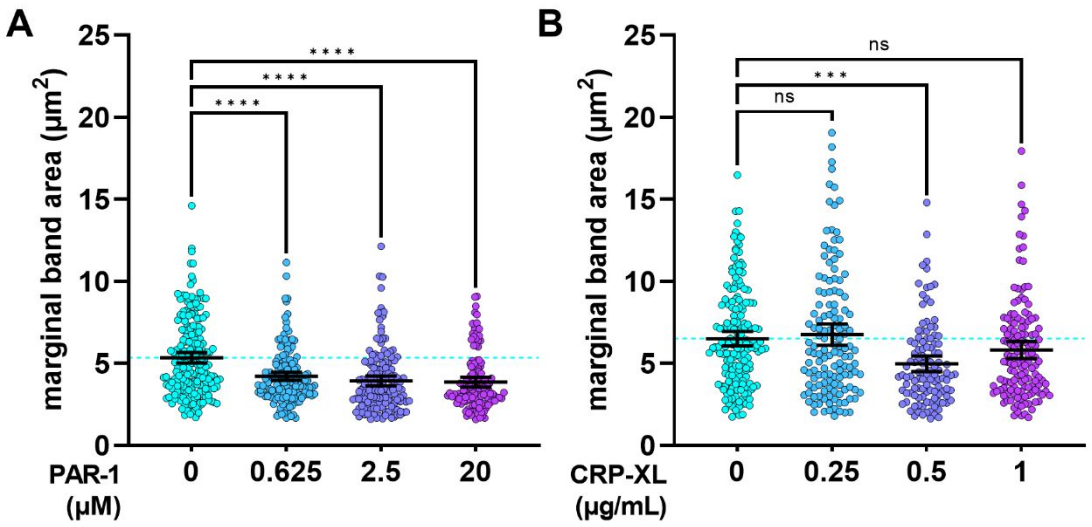

Supplemental Figure 5: Compression of marginal band area in PAR1- and GPVI-activated platelets. Platelets were incubated with vehicle or increasing doses of PAR-1 ap or CRP-XL (B). Marginal band area was determined based on the delineation by the alpha-tubulin immunofluorescent staining of the ring structure in the middle Z-slice. Data shown are derived from platelets from 3 independent healthy control donors (PAR1 0 μM, n=208; PAR1 0.625 μM, n=166; PAR1 2.5 μM, n=157; PAR1 20 μM, n=128; CRP-XL 0 μg/mL, n=179; CRP-XL 0.25 μg/mL, n=137; CRP-XL 0.5 μg/mL, n=113; CRP-XL 1.0 μg/mL, n=139). Bars represent means and 95% confidence interval. *** p<0.001, **** p<0.0001 by 1-way ANOVA with Dunnett's post hoc test for multiple comparison.

Supplemental Figure 6

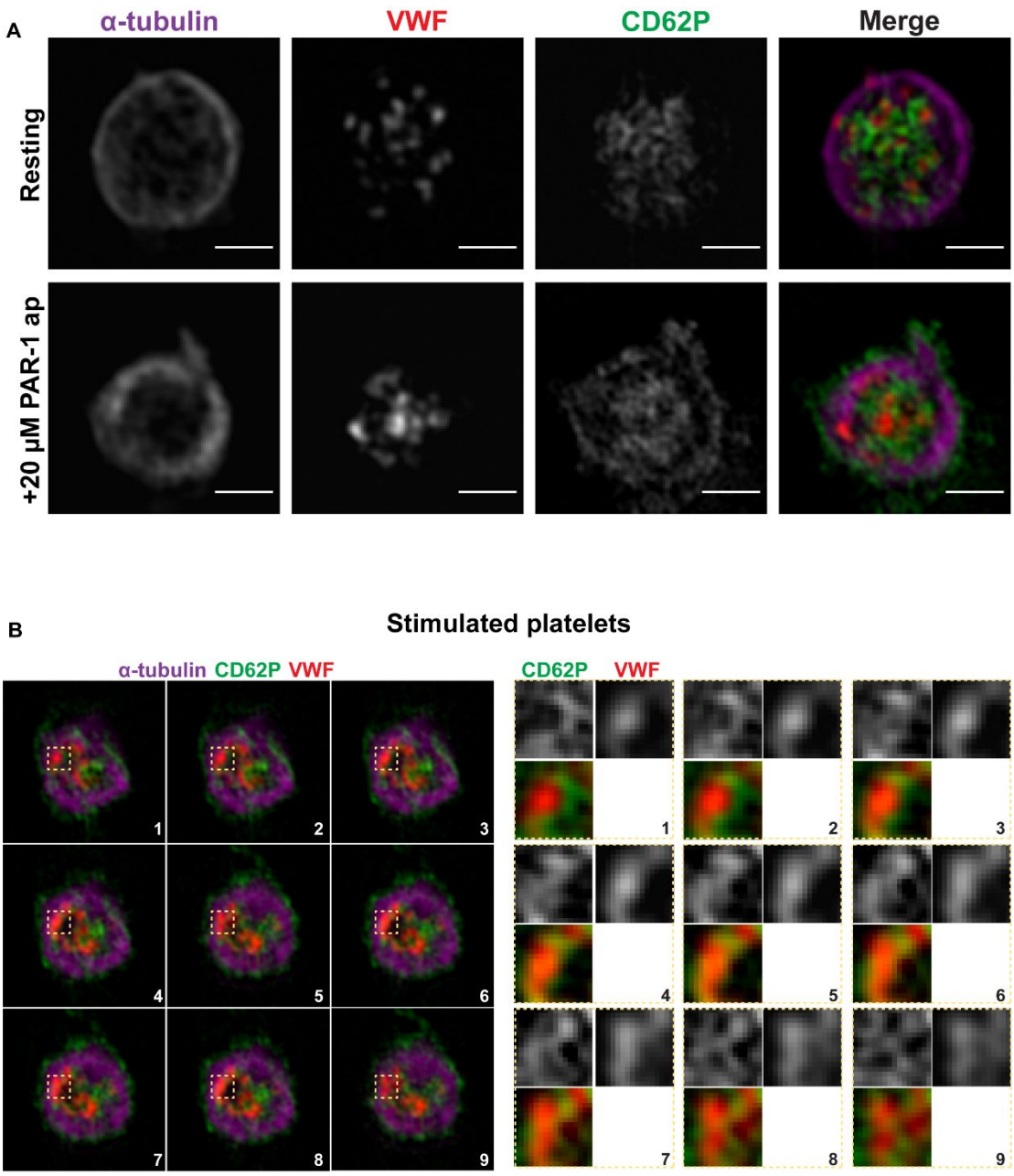

Supplemental Figure 6: 3D VWF localization in stimulated platelets. Platelets stimulated with 20 µM PAR-1 ap were stained for CD62P (green), VWF (red, DAKO) and α-tubulin (magenta) and compared to resting platelets (A). Serial planes of a zoom-in image are shown with granule details on the right (yellow squares) to illustrate 3D localization of CD62P and VWF (B). Scale bar represents 1 µm.

Supplemental Figure 7

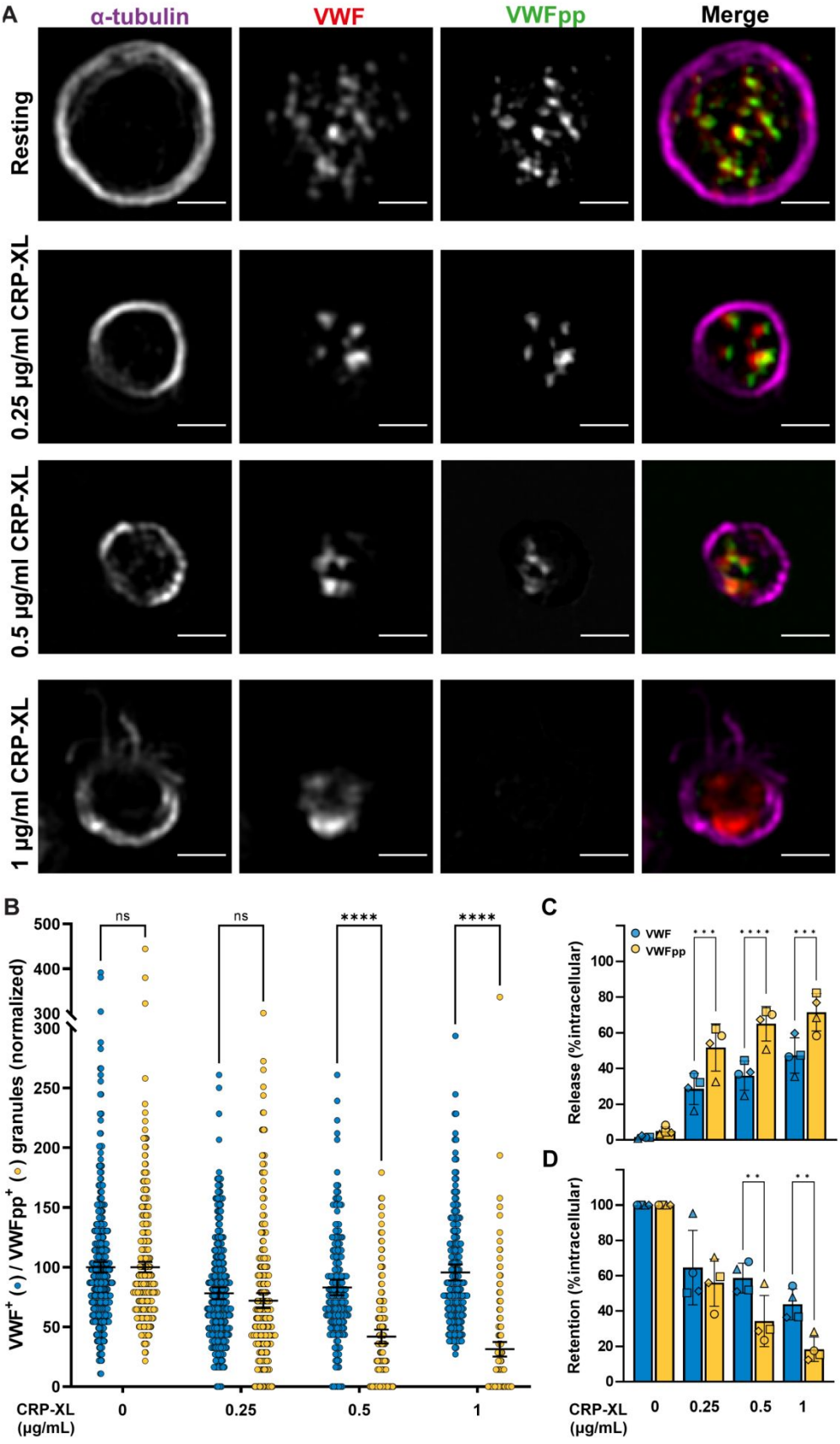

Supplemental Figure 7: Dose-response release of VWF and VWFpp. Platelets were stimulated with 0-1 µg/ml CRP-XL and stained for α-tubulin, VWF (CLB-RAg20) and VWFpp (A). Representative single plane zoom-in images are shown. Scale bar represents 1 µm. (B) VWF and VWFpp release were assessed by quantification of their residual levels in platelets normalized to resting platelets. N=498, 305, 187 and 191 respectively. Counts are pooled from 3 independent healthy donors. The release (C) and retention (D) of VWF and VWFpp in CRP-XL stimulated platelets was measured by ELISA and normalized to resting intracellular content. Symbols represent 4 healthy donors (N=4). Statistical analysis was two-way ANOVA with Sidak multiple comparisons test and significance levels of ** = $p<0.01$,*** = $p<0.001$, **** = $p<0.0001$. Data is presented as mean with 95% confidence interval.

Supplemental Figure 8

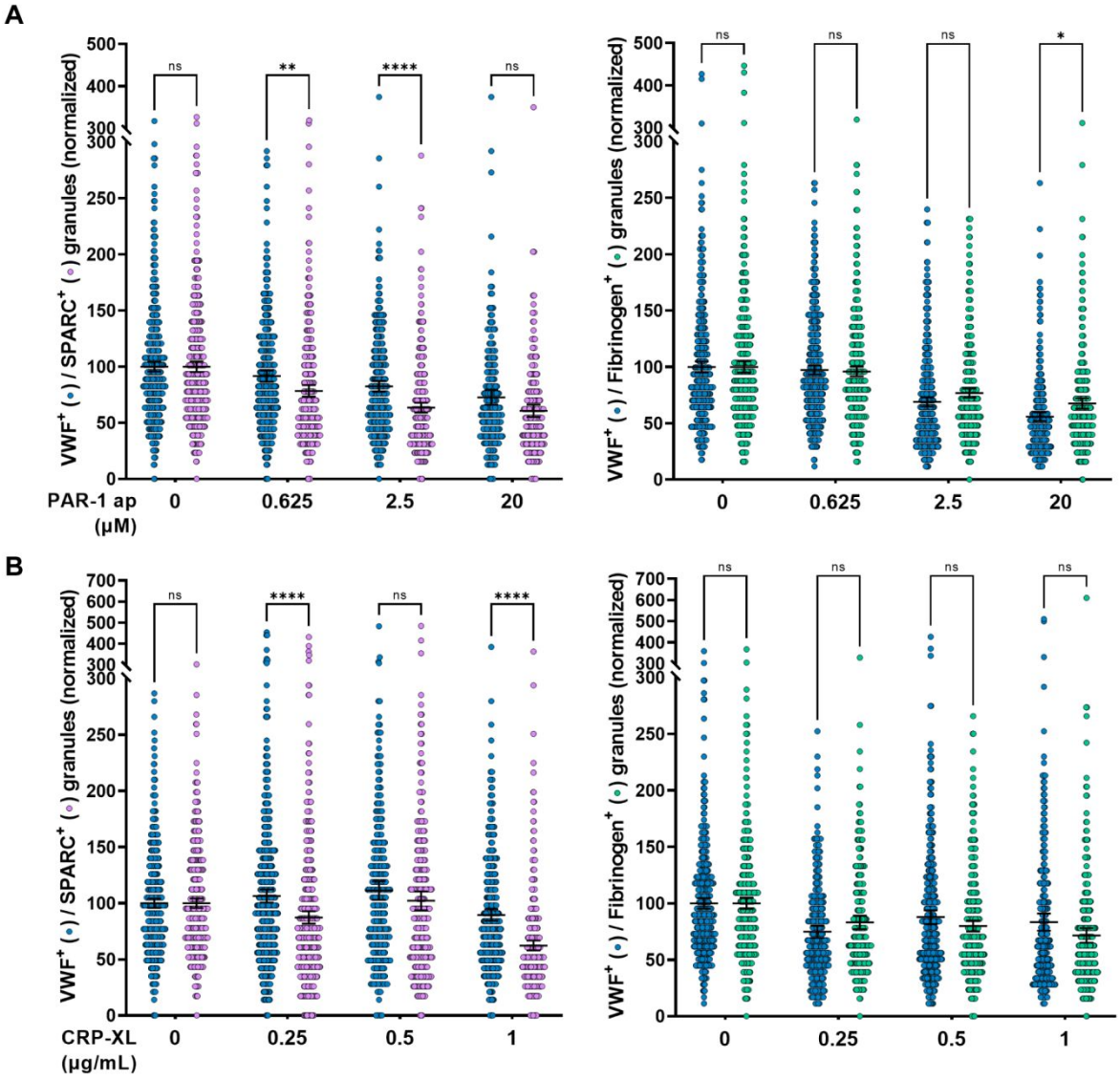

Supplemental Figure 8: Dose-response release of VWF compared to SPARC and Fibrinogen. Platelets were stimulated with 0-20 μM PAR-1 ap (A) or 0-1 μg/ml CRP-XL (B). VWF (blue), SPARC (pink) and fibrinogen (green) release was assessed by quantification of their residual levels in platelets normalized to resting platelets. (**SPARC** PAR1 0 μM, n=512; PAR1 0.625 μM, n=376; PAR1 2.5 μM, n=355; PAR1 20 μM, n=218; CRP-XL 0 μg/mL, n=512; CRP-XL 0.25 μg/mL, n=480; CRP-XL 0.5 μg/mL, n=263; CRP-XL 1.0 μg/mL, n=401) (**Fibrinogen** PAR1 0 μM, n=549; PAR1 0.625 μM, n=499; PAR1 2.5 μM, n=437; PAR1 20 μM, n=342; CRP-XL 0 μg/mL, n=430; CRP-XL 0.25 μg/mL, n=255; CRP-XL 0.5 μg/mL, n=355; CRP-XL 1.0 μg/mL, n=292)
* = p<0.1, ** = p<0.01, **** = p<0.0001, as analyzed by two-way ANOVA with Sidak multiple comparison test. Data presented as mean with 95% confidence interval.

Supplemental Figure 9

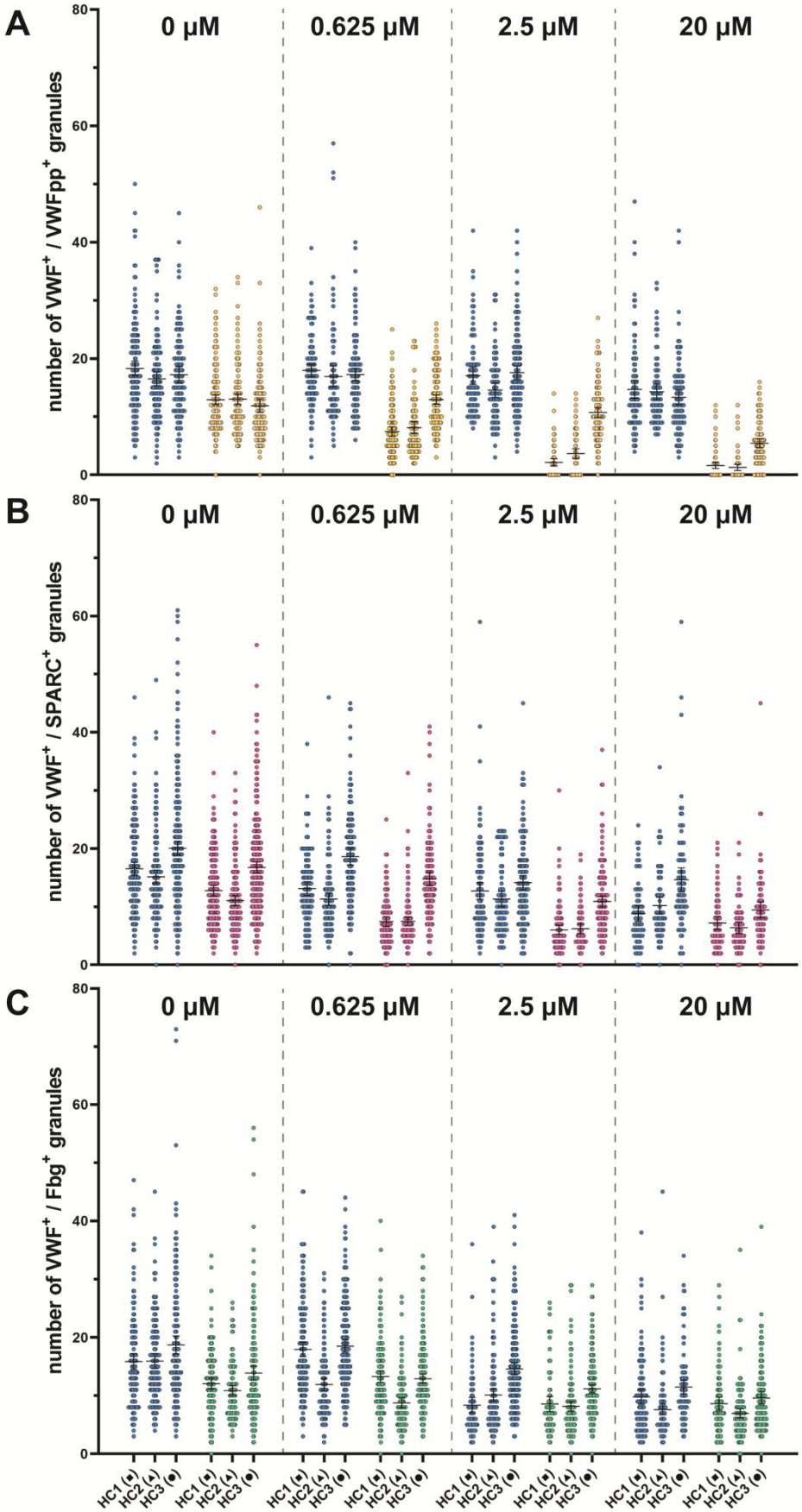

Supplemental Figure 9: Healthy donor variation in dose-response release. Platelets of healthy donors were stimulated with 0-20 µM PAR-1 ap and imaged by SIM. Absolute counts of VWF and VWFpp (A), SPARC (B) and fibrinogen (C) positive granules are shown per donor. The symbol for each individual donor corresponds to the one that is used in Supplemental Figure 4.

Supplemental Figure 10

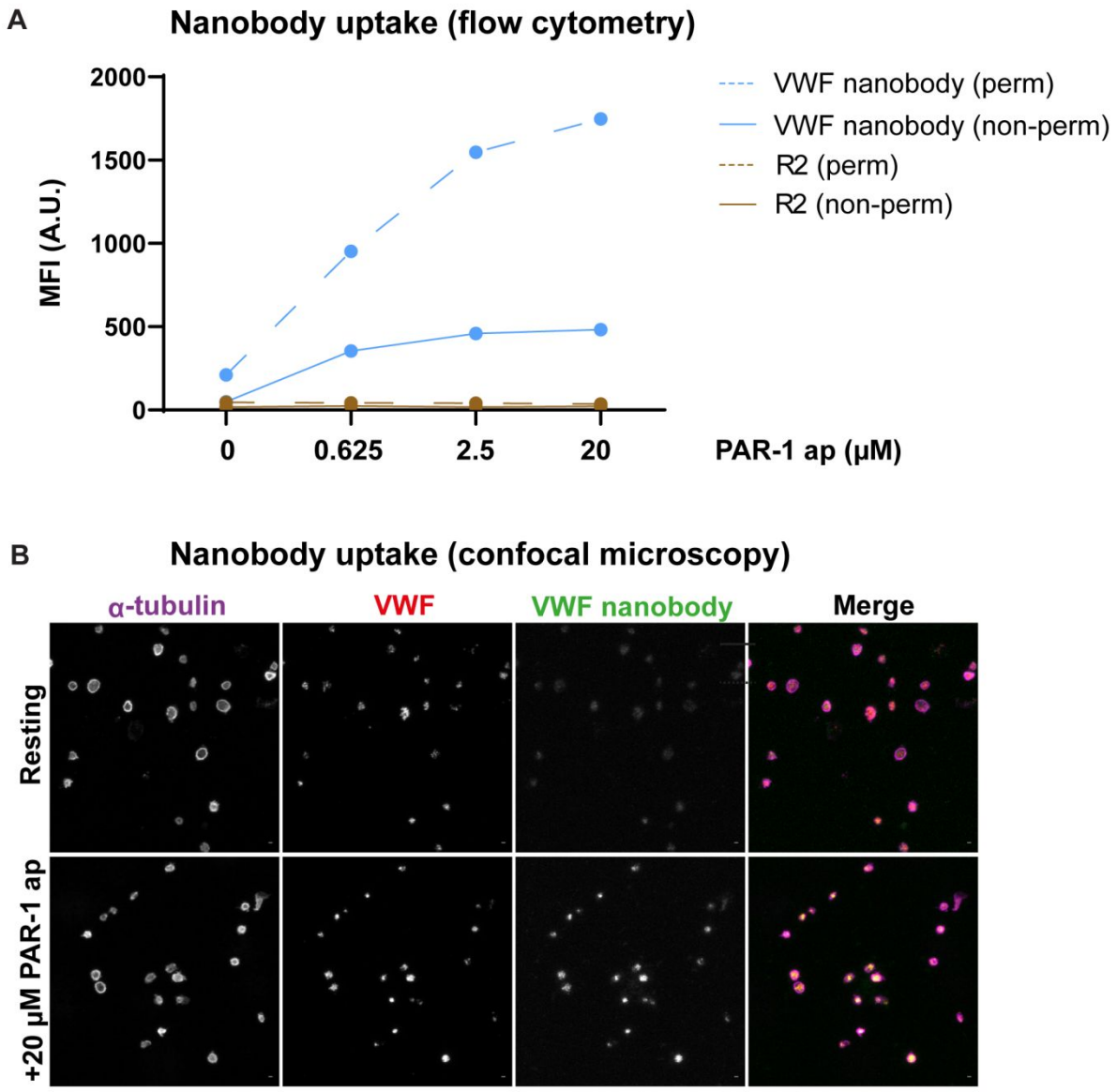

Supplemental Figure 10: VWF nanobody bulk uptake in platelets. Platelets were stimulated for 30 minutes with 0-20 μM PAR-1 in the presence of 1 μg/ml VWF nanobody or R2 control nanobody and were analyzed for nanobody uptake by flow cytometry (A) and confocal microscopy (B).